

# Nanocrystal-Enabled Perovskite Heterojunctions in Photovoltaic Applications and Beyond

Brian M. Wieliczka, Severin N. Habisreutinger, Kelly Schutt, Jeffrey L. Blackburn,\* and Joseph M. Luther\*

Heterojunctions are used to tailor the properties of semiconductors in optoelectronic devices, yet for emerging devices composed of metal halide perovskites, fabricating perovskite/perovskite heterojunctions has proved challenging due to solvent incompatibilities and rapid homogenization due to ion migration. Recent studies have demonstrated various strategies for using perovskite nanocrystals as a component to fabricate perovskite/perovskite heterojunctions, either with a perovskite thin film or a second nanocrystal layer. Heterojunctions such as these can impart many advantages of both bulk and nanocrystalline perovskite morphologies. This perspective focuses on recent developments of solution-processed perovskite heterojunctions for solar cells and novel optoelectronic devices, in particular, highlighting the demonstrated and potential advantages of nanocrystal-enabled fabrication strategies. A central tenet of this perspective is that the synthesis and dispersion of perovskite nanocrystals in non-polar organic solvents offers a key processing advantage over traditional perovskite precursor solutions in polar solvents since the former allows for layer-by-layer deposition without dissolving an underlying perovskite film or crystal. This processing advantage, coupled with nanocrystal size control and ligand chemistry, enables perovskite heterojunctions with highly tunable optical and electrical properties. Such heterojunctions may enable disruptive technological advances in broad classes of devices such as solar cells, photodetectors, sensors, and (in) coherent photon sources with tunable polarization.

## 1. Introduction


Metal halide perovskites (MHPs) and their related structures are unique semiconductor systems embodying many of the characteristics of both inorganic and organic semiconductors.<sup>[1]</sup> Like III–V materials, MHP thin films are crystalline with long-range order and excellent optoelectronic properties, leading to high voltages in photovoltaic cells,<sup>[2]</sup> slow hot-carrier cooling,<sup>[3]</sup> and novel applications such as optical cooling.<sup>[4]</sup> Like organic semiconductors, MHP films promise to be lightweight, solution-processable, inexpensive, and flexible.<sup>[5,6]</sup> Although MHP materials share many of the beneficial properties of both organic and inorganic semiconductors, forming stable perovskite/perovskite heterojunctions has remained a unique and elusive challenge for MHPs specifically.

Much of the success of III–V materials in modern-day optoelectronics arises from the formation of heterojunctions or heterostructures where abrupt semiconductor/semiconductor interfaces allow for a high degree of control over the flow of charge carriers. This foundational concept of a heterostructure formed part

of the basis of the 2000 Nobel Prize in Physics awarded for high-speed optoelectronics.<sup>[7]</sup> Heterostructures underlie the major functionality of lasers, transistors, diodes, certain photovoltaics, and related technologies based on III–V semiconductors. In such applications, the heterostructure enables better control over the optical and electronic properties through strategies such as confinement of carriers, tuning of electronic states, and energy level offsets to direct charges. Heterostructure formation can also impact mechanical properties, especially when considering the variability of interfacial bonding discussed below. Such impacts are outside of the scope of this perspective but have been recently studied.<sup>[8]</sup> Applying this vast existing knowledge base to MHP-based optoelectronic materials could yield a completely new category of applications leveraging MHPs' unique phonon structure,<sup>[3,9–11]</sup> strong spin-orbit coupling,<sup>[12–17]</sup> tunable chiroptical properties,<sup>[18–24]</sup> magnetic properties,<sup>[25–27]</sup> and coupled ionic/electronic conductance mechanisms.<sup>[28–30]</sup>

B. M. Wieliczka, S. N. Habisreutinger, K. Schutt, J. L. Blackburn, J. M. Luther  
National Renewable Energy Laboratory  
Center for Hybrid Organic Inorganic Semiconductors for Energy  
15013 Denver West Parkway, Golden, CO 80401, USA  
E-mail: jeffrey.blackburn@nrel.gov; joey.luther@nrel.gov

J. M. Luther  
Renewable and Sustainable Energy Research Institute (RASEI)  
University of Colorado  
Boulder, CO 80309, USA

 The ORCID identification number(s) for the author(s) of this article can be found under <https://doi.org/10.1002/aenm.202204351>.

© 2023 The Authors. Advanced Energy Materials published by Wiley-VCH GmbH. This is an open access article under the terms of the Creative Commons Attribution License, which permits use, distribution and reproduction in any medium, provided the original work is properly cited.

DOI: 10.1002/aenm.202204351

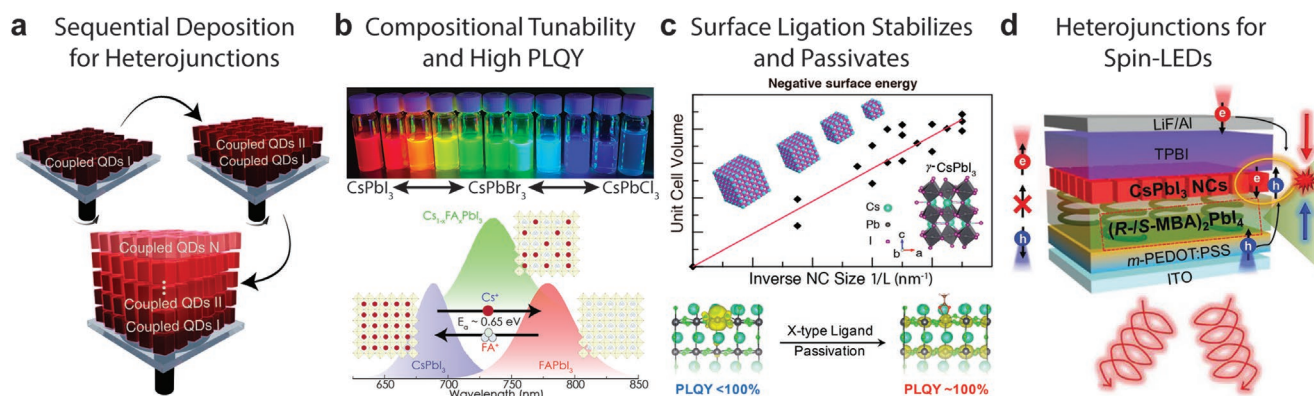


**Figure 1.** Opportunities for heterojunctions using MHP NCs taking advantage of a) sequential deposition, b) tunable composition and high photoluminescence quantum yield, c) stabilization of surfaces using strain and ligands, and d) manipulation of charge carrier spin. Panel (a) adapted with permission under the terms of the CC-BY license.<sup>[50]</sup> Copyright 2019, the authors, published by Nature Springer. Panels (b) and (c) adapted with permission.<sup>[36,37,48]</sup> Copyright 2018 and 2020, American Chemical Society. Panel (d) adapted with permission.<sup>[24]</sup> Copyright 2021, The American Association for the Advancement of Science.

We present here a perspective on the many opportunities where colloidal perovskite nanocrystals (PNCs) can be used to produce functional interfaces, control composition gradients, and regulate doping gradients, potentially leading to new paradigms in device design. Due to their unique properties, PNCs can be used to fabricate heterostructures with other PNCs, thin film MHPs, or other semiconductors. Colloidal PNCs offer several key advantages for fabricating heterostructures. First, PNCs are suspended in nonpolar organic solvents, thus allowing for direct deposition of PNC solutions onto MHP thin films (**Figure 1a**) without risking solvent damage to the underlying film commonly caused by more polar solvents. Secondly, PNCs can intercalate into small areas or porous films, enabling intimate contact between the PNCs and individual grains in the polycrystalline thin films, especially along grain boundaries. Third, PNCs offer additional advantages such as high luminescence efficiency (Figure 1b),<sup>[31–36]</sup> highly tunable composition (Figure 1b),<sup>[37–43]</sup> passivating effects (Figure 1c),<sup>[44–47]</sup> crystallographic stabilization through surface strain<sup>[48]</sup> (Figure 1c), ease of incorporation of dopants or surface species,<sup>[49]</sup> all while providing adequate to modest charge transport properties, such as the ability to withstand and utilize injected carriers with specific spin character (Figure 1d).<sup>[50–56]</sup> Additionally, the brightness of PNCs can be exploited while using a conventional MHP as a matrix to improve passivation.<sup>[57]</sup> This highlights the many different ways to combine PNCs and MHP films for advanced functionality.

PNC-enabled heterojunctions have the potential to not only improve device performance but also to retain these improvements against the stresses of operating conditions due to their inherent stabilization by surface ligands. For example, PNC ligands have been shown to slow certain ion migration within the film.<sup>[50,58]</sup> These hydrophobic ligands also serve to improve the long-term resilience of the MHPs against moisture-induced degradation. While the sequential deposition of different types of PNCs already results in heterostructures,<sup>[50,58–60]</sup> the conditions of PNC deposition and post-deposition treatments can further lead to ion incorporation or formation of different phases responsible for performance improvements.<sup>[44–46]</sup>

We will focus first on the use of PNCs in heterojunctions specifically in solar cells and subsequently discuss strategies for the use of PNCs in heterojunctions for emerging applications such as neuromorphic computing and quantum information processing.

## 2. Fundamental Properties of Semiconductor Heterojunctions

Heterostructures of single crystalline materials like III–V semiconductors are formed through epitaxial interfaces where repeating atomic bonds and crystallographic orientation persist despite the composition change (**Figure 2a**). The lattice constants of each component are a critical parameter to minimizing interfacial disorder. With high lattice mismatches, increased strain causes the breakdown of the epitaxial interface (Figure 2b) leading to less well-defined interfaces with voids and/or interfacial charges. Perfection of the epitaxial interface has not been required for high-performance thin-film photovoltaics like CdTe and CIGS where interfaces between oxides and the semiconductors are formed by brute force deposition onto an existing layer without much concern for the epitaxial coherence of adjacent layers. This concept has carried over to perovskite devices where a typical high-performance solar cell may have four or more material interfaces with no consideration of lattice coherency.

The majority of MHP interfaces are similar to the random interface shown in Figure 2b and/or the van der Waals interface shown in Figure 2c. Perovskite/perovskite epitaxial interfaces have been demonstrated in various morphologies of note (shown in Figure 2d),<sup>[62,63]</sup> but these epitaxial interfaces are not yet the norm for optoelectronic devices and many MHP interfaces are more likely to be random (Figure 2e), especially for PNCs where the ligand shells around the PNCs are involved. The increased disorder shown in Figure 2b,e, while not ideal, can still be tolerated in MHPs due to defect screening and defect-tolerant properties.<sup>[64–66]</sup> Rather than perfect epitaxial interfaces, layers can frequently exhibit electronic coupling

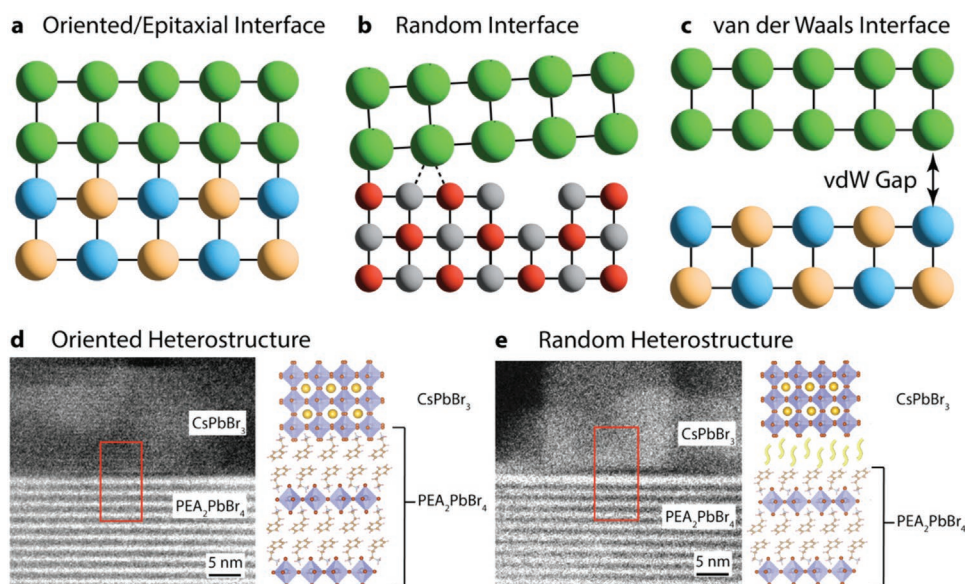


**Figure 2.** Depiction of hypothetical heterostructure interfaces where a) an oriented epitaxial interface is shown with matched lattice constants and coherent atomic bonding across the interface. b) A random interface is shown where some atomic bonds are present, but the substantial lattice constant mismatch prevents homogeneous crystallinity. This interface may possess voids or dangling bonds and interfacial trap states. c) A van der Waals (vdW) interface where no atomic bonding is present, but the materials are coupled through the vdW gap which is narrow enough to enable tunneling. (d) and (e) show an oriented heterostructure and random heterostructure, respectively, between  $\text{CsPbBr}_3$  and  $\text{PEA}_2\text{PbBr}_4$ . In panel (e), unordered molecules are depicted between the two components preventing proper epitaxy. d,e) Adapted with permission.<sup>[61]</sup> Copyright 2022, Springer Nature Limited.

through little to no chemical bonding where van der Waals interactions dominate. Other perovskite interfaces have shown mixed character where grains may form with chemical bonding adjacent to voids, leading to a messier interface that remains good enough for high-performance device applications where screening or defect tolerance is present in MHPs, and these types of interfaces will be the major focus of this article.<sup>[67]</sup>

A primary goal of semiconductor heterojunctions is to establish 1) precise interfacial energy level alignments (**Figure 3a**) that facilitate the flow of energetic species (e.g., excitons, electrons, holes) in specified directions and 2) tailored optical properties (**Figure 3b**)<sup>[68]</sup> that enable broad- or narrow-band absorption and/or emission in desired spectral regions. In MHP semiconductors, changes to the identities of A-, B-, and

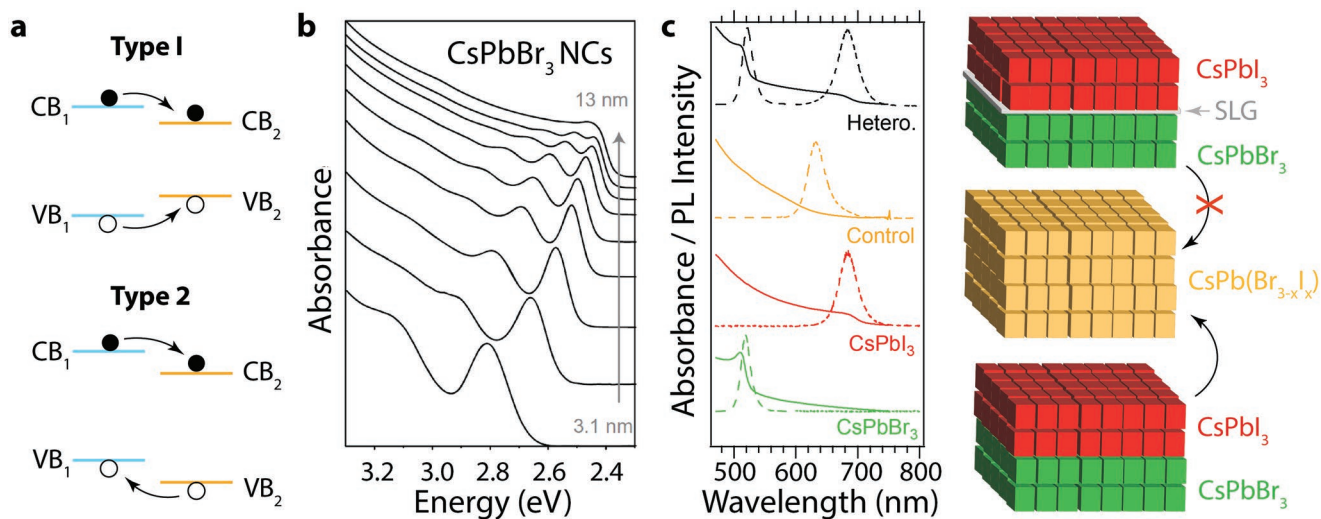


**Figure 3.** a) Schematics of type I and type II interfacial band alignments, demonstrating the expected energy and charge transfer pathways, respectively, enabled by these alignments. b) Size-tunable excitonic transitions of PNCs can modulate the optoelectronic properties of a heterojunction. From Akkerman et al.<sup>[68]</sup> Reproduced with permission.<sup>[68]</sup> Copyright 2022, AAAS. c) Single-layer graphene (SLG) ion blocking layers can eliminate interfacial ion diffusion and homogenization over 30 days in ambient conditions, demonstrated in this study for a  $\text{CsPbI}_3/\text{CsPbBr}_3$  heterojunction (HJ) through optical absorption and photoluminescence and schematically depicted in panel (d). Panel (c) adapted under the terms of the C-CBY license.<sup>[69]</sup> Copyright 2023, the authors, published by American Chemical Society.



X-site components provide a large pallet of optoelectronic tunability. A compelling property of semiconductor NCs in general, including perovskite NCs, is the ability to use NC size as a sensitive knob for tuning both optical absorption and the energetic positions of the conduction band minimum (CBM) and valence band maximum (VBM) to tailor the heterostructure's optical and electronic properties (Figure 3). PNCs also have the added benefit of incorporating a huge variety of surface ligands with additional optical properties and molecular orbitals. To understand the potential impacts of this broad tunability, we turn to a more detailed discussion of heterostructure interfacial band alignment and optical properties.

Figure 3a shows schematics of type I and type II interfacial band alignments, the most common alignments for semiconductor heterojunctions. In type I heterojunctions, the CBM and VBM of a small bandgap semiconductor are farther away from and closer to the vacuum, respectively, relative to a large bandgap semiconductor. This type of band alignment provides a thermodynamic driving force for charge carriers in both bands (CB<sub>1</sub>, VB<sub>1</sub>) of the large bandgap semiconductor to be transferred to the bands (CB<sub>2</sub>, VB<sub>2</sub>) of the small bandgap semiconductor, thus favoring interfacial energy transfer. The exact mechanism of this interfacial energy transfer depends on the interface and can involve either simultaneous (concerted) or sequential transfer of the electron and hole. In type II band alignment, often termed “staggered” band alignment, both the CBM and VBM of one semiconductor are closer to vacuum than that of the other semiconductor. This type of band alignment provides a thermodynamic driving force for interfacial charge separation, whereby one carrier can favorably transfer from the originating semiconductor to the other thus separating the charges from each other.<sup>[70]</sup>

These band alignments help to define the electrical properties and processes of both the ground state and excited state of

semiconductor heterojunctions. In the ground state, interfacial band alignment and ground-state majority carrier density (and associated Fermi level,  $E_f$ ) combine to determine the ground-state charge transfer, Fermi level equilibration, and interfacial band bending that occurs during heterojunction formation. In the excited state, band alignment and band bending dictate the direction, rate, and efficiency of interfacial charge/energy transfer.

UV and X-ray photoelectron spectroscopy (UPS and XPS) are crucial tools for determining the VBM and work function ( $\phi$ ) of semiconductors, including MHPs, and can be used to estimate interfacial band alignments. It is important to note that the majority carrier type and density, and hence  $E_f$ , are not always easy to determine or predict for MHPs. In some cases, these properties have been observed to depend sensitively on the substrate in contact with the perovskite.<sup>[71]</sup> This sensitivity results in some inherent uncertainty in predicting interfacial band bending in MHP heterojunctions. However, thickness-dependent photoelectron spectroscopy measurements have been used in many MHP heterojunctions to extract interfacial band bending profiles<sup>[50,72]</sup> and this technique has also been effective for the PNC heterojunctions shown in Figure 4c. Excited state dynamics can also be utilized to verify the determined band alignment. As an example, in Figure 4d, and the associated reference,<sup>[50]</sup> transient absorption was performed incident on each direction of the heterostructure to track the impact of the band alignment via the time-dependent movement and bleaching characteristics of photogenerated carriers.

The optical properties of semiconductor heterojunctions can be tuned by the properties of both the individual semiconductors and the heterojunction itself. In the simplest case, optical absorption is a linear superposition of the spectra of each individual semiconductor. The optical emission (luminescence) depends sensitively on the interfacial band alignment.

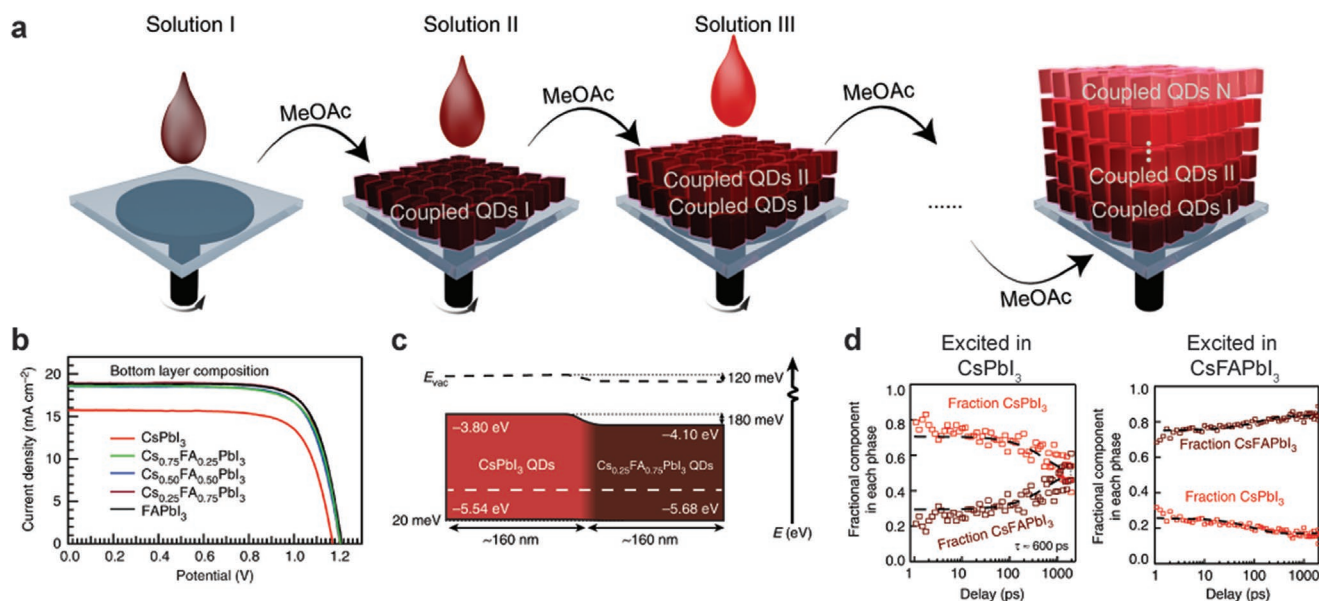


**Figure 4.** a) Perovskite nanocrystal deposition and ligand exchange method can be used to build up a film with varying compositions. Through selecting the best bottom layer composition, b) the solar cell performance can be optimized as a c) result of differing band offsets. d) Selective charge transfer was found to be responsible for this increase in performance through transient absorption experiments. Adapted under the terms of the CC-BY license.<sup>[50]</sup> Copyright 2019, the authors, published by Nature Springer.

For example, energy transfer in type I heterojunctions can potentially enhance (deplete) the emission of the small (large) bandgap semiconductor, whereas interfacial charge separation in type II heterojunctions can quench the emission of both semiconductors. In some heterojunctions, interfacial hybridization of orbitals from each semiconductor can give rise to new hybrid states with distinct optical absorption and/or emission. For example, several heterojunctions between monolayer transition metal dichalcogenides (TMDCs) and other TMDCs or small molecules give rise to low-energy interfacial charge transfer excitons with varying absorption and emission intensities.<sup>[70]</sup> Analogous charge transfer excitons have also been observed in several 1D hybrid organic/inorganic metal halide semiconductors and are attributed to hybrid states at the interface between the small molecule and metal halide framework.<sup>[73,74]</sup>

We emphasize that the above discussion assumes a relatively abrupt heterojunction between two semiconductors. Creating and retaining such an abrupt perovskite/perovskite heterojunction is challenging due to the MHPs' low formation enthalpy, their solubility, and high ionic mobility.<sup>[75]</sup> It is therefore very difficult to fabricate a heterojunction through sequential solvent-based deposition of two or more perovskites, as subsequent layer deposition results in re-dissolution of the underlying MHP layer(s). Furthermore, even when such processing challenges do not prohibit the formation of an ostensibly abrupt heterojunction, facile ion diffusion can rapidly homogenize the interface and destroy the desired electrical and optical properties. Such issues are particularly problematic for interfaces between MHPs with different halide species since halide diffusion has especially low activation energy in MHPs.

There are several common approaches to overcoming the challenges discussed directly above. Non-solution processing methods, such as film transfer<sup>[76]</sup> or vapor deposition,<sup>[77,78]</sup> permit sequential deposition of MHPs, but rely on at least one layer to be compatible with such processing methods. Another method particularly useful in creating a very thin second layer is to only deposit A-site molecules, for example, and rely on the BX components of the first layer to create a surface heterostructure via chemical transformation of the surface. This approach has been commonly applied to surfaces of film for photovoltaics, where a larger molecule can form a 2D perovskite surface layer.<sup>[79–82]</sup> The formation of 3D/2D heterojunctions has boosted MHP-based solar cell performance by facilitating both the passivation of surface defects and suppression of interfacial recombination.<sup>[83–85]</sup> In such cases the higher bandgap 2D layer must typically be kept thin so that charge carriers can tunnel through the layer for extraction.

With each processing approach discussed above, interfacial ion diffusion can still be a problem. However, a recent study demonstrated that ultra-thin ion diffusion barriers can mitigate this issue (Figure 3c,d).<sup>[69]</sup> In this study, a single layer of graphene eliminated the rapid  $I^-/Br^-$  mixing that otherwise occurs across a  $CsPbI_3/CsPbBr_3$  heterojunction without graphene. The optical properties of the heterojunction without graphene represented a homogeneous  $CsPb(Br_{1-x}I_x)_3$  layer, whereas the heterojunction with single-layer graphene retained the desired abrupt heterojunction and the optical properties of each individual NC layer. This strategy can be applied across a broad array of perovskite heterojunctions that include both NC layers and per-

ovskites of other dimensionalities and can also be expanded to other intervening layers, such as hexagonal boron nitride and transition metal dichalcogenide layers.

### 3. Differences in Solvent Dispersibility allow Heterojunction Fabrication

Differences in PNC dispersibility compared to MHP salt precursors enables the fabrication of heterostructures within films. PNCs are ligated with long-chain aliphatic ligands, required for their synthesis and stabilization, and which allow for the PNCs to be dispersed and processed using nonpolar solvents which would not otherwise dissolve MHP salts. The drawback of these ligands is that their insulating nature results in reduced or suppressed charge transport when deposited in a film. Therefore, for PNC solar cell fabrication, a solid-state ligand exchange is typically performed (Figure 4a). This ligand exchange replaces long-chain oleate ligands with short-chain acetate ligands, reducing their dispersibility in nonpolar solvents while increasing charge mobility in the film.<sup>[86]</sup> In all-PNC solar cells, this solid-state ligand exchange is used to deposit sequential layers of PNCs to build up an optically thick absorber layer (e.g.,  $CsPbI_3$ ). This strategy has also been applied to fabricate PNC heterojunctions such as  $CsPbI_2Br/CsPbI_3$ ,  $Cs_{0.25}FA_{0.75}PbI_3/CsPbI_3$ , and  $CsPbI_3/FAPbI_3$ .<sup>[50,59,60]</sup>

As demonstrated by Zhao et al., a PNC heterojunction within *n-i-p* solar cells improves the ability to separate charge carriers, resulting in an increase in the short-circuit current density ( $J_{SC}$ ) and increased charge transfer measured in transient absorption (TA) experiments (Figure 4b–d).<sup>[50]</sup> The built-in potential within the absorber film increased the  $J_{SC}$  by 20% from 15.75 mA cm<sup>-2</sup> for  $CsPbI_3$  to 18.91 mA cm<sup>-2</sup> for  $Cs_{0.25}FA_{0.75}PbI_3/CsPbI_3$  PNC solar cells. This enhancement resulted from the charge-separating heterostructure, as demonstrated by probing the transient absorption signal when exciting through either the  $Cs_{0.25}FA_{0.75}PbI_3$  or  $CsPbI_3$  PNCs (Figure 4d). Excitation into  $CsPbI_3$  showed that charge carriers are transferred to the  $Cs_{0.25}FA_{0.75}PbI_3$ , whereas excitation into the  $Cs_{0.25}FA_{0.75}PbI_3$  did not result in electron transfer, confirming an increase in charge carrier collection efficiency through establishing a built-in electric field and directional flow of charges regardless of generation location. In addition to efficiency increases,  $CsPbI_3/FAPbI_3$  PNC heterostructures have been shown to increase PNC solar cell stability.<sup>[60]</sup>

Varying the A-site across PNC heterostructures has also been reported by Park et al.<sup>[58]</sup> and Li et al.,<sup>[60]</sup> demonstrating the robustness of this strategy for creating stable interfaces. While Li et al. fabricated *n-i-p* solar cells, similar to Zhao et al., they deposited the PNCs in the opposite order: Cs-rich PNCs first with the FA-rich composition on top. In both cases, the PCE of the heterostructured solar cell is better than the PNC solar cells fabricated from either PNC composition alone, primarily due to an increase in the  $J_{SC}$ . This suggests that the formation of a built-in field and the consequently enhanced charge extraction is responsible for the improved PNC solar cell performance, independent of the sequential arrangement of the heterojunction's PNCs.<sup>[50]</sup> Further studies of these heterostructures are needed to understand this difference and could enable greater

control of the photogenerated charge carriers in PNC solar cells and other optoelectronic devices. Most of these studies indicate that ion migration can be avoided on the A-site more readily than when compared to heterostructures with different halides.

The same strategy has been used to fabricate MHP thin film/PNC heterojunctions with improved charge collection (shown later in Figure 7).<sup>[59]</sup> In this case, the PNCs were deposited on top of a 3D MHP thin film, which does not dissolve because the PNCs are dispersed in a non-polar solvent that only interacts with their ligands, rather than polar solvents used to solvate MHP component salts. This strategy was successfully employed to create a graded interface between bulk CsPbI<sub>2</sub>Br and CsPbI<sub>3</sub> PNCs. Compared to the bulk by itself,  $J_{SC}$  was improved by the graded interface with the NCs and hence the power conversion efficiency (PCE) increased from 13.45% to 14.45%, which was the highest-reported PCE for an all-inorganic MHP solar cell at the time.<sup>[59]</sup>

#### 4. Charge Carrier Recombination at Charge Transport Layers

Perovskite solar cells are heavily dependent on charge carrier selective contact layers and passivation of the contact layer/MHP thin film interface.<sup>[88]</sup> Since MHPs' first use in solar cells,<sup>[89]</sup> enormous efforts have focused on MHP compositional control,<sup>[90,91]</sup> crystallization,<sup>[92]</sup> and structure across various dimensionalities.<sup>[38,93–106]</sup> Key to the rapid rise of the MHP single junction solar cell efficiency from 3.8% in 2009<sup>[89]</sup> to 25.7% in 2022<sup>[107]</sup> is reduced interfacial losses and improved transport layers,<sup>[108]</sup> which are typically low-conductivity, wide-gap semiconductors. The successful management of charge carriers at interfaces highlights the

promise of using perovskite/perovskite heterojunctions to simultaneously improve the open circuit voltage ( $V_{OC}$ ) by reducing surface recombination and increase the  $J_{SC}$  by enhancing charge extraction.

Steady-state photoluminescence techniques have helped to identify sources of  $V_{OC}$  losses in bulk MHP and PNC solar cells.<sup>[31,87]</sup> Bulk *p-i-n* MHP solar cells without additional interfacial passivation experience significant non-radiative interface recombination as a result of contact with most charge transport layers.<sup>[87]</sup> Quasi-Fermi level splitting (QFLS) mapping (Figure 5a) demonstrates that non-radiative interfacial recombination limits the  $V_{OC}$ , as reflected by significantly decreased QFLS when the bulk MHP is in contact with PTAA and C<sub>60</sub> (Figure 5a,c).<sup>[87]</sup> In contrast, the  $V_{OC}$  of PNC *n-i-p* solar cells is not limited by increased interfacial charge carrier recombination (Figure 5b,c).<sup>[31]</sup>

Taken together, these results indicate that the passivation of the MHP/charge transport layer interface with PNCs can enhance  $V_{OC}$  in MHP solar cells.<sup>[44–46]</sup> The majority of recombination losses in MHP solar cells tends to occur at the exposed interfaces,<sup>[109,110]</sup> largely attributed to trap states associated with interfacial defects such as vacancies.<sup>[111,112]</sup> Since interfaces between MHP thin films and PNCs do not induce additional recombination losses, the incorporation of PNCs at the interfaces of bulk MHP solar cells could reduce the QFLS losses in the solar cell, thereby improving the  $V_{OC}$  and performance.

#### 5. Charge Carrier Extraction at Interfaces

While passivating defects is critical to obtaining high  $V_{OC}$ , solar cell performance can also be limited by the inability to extract

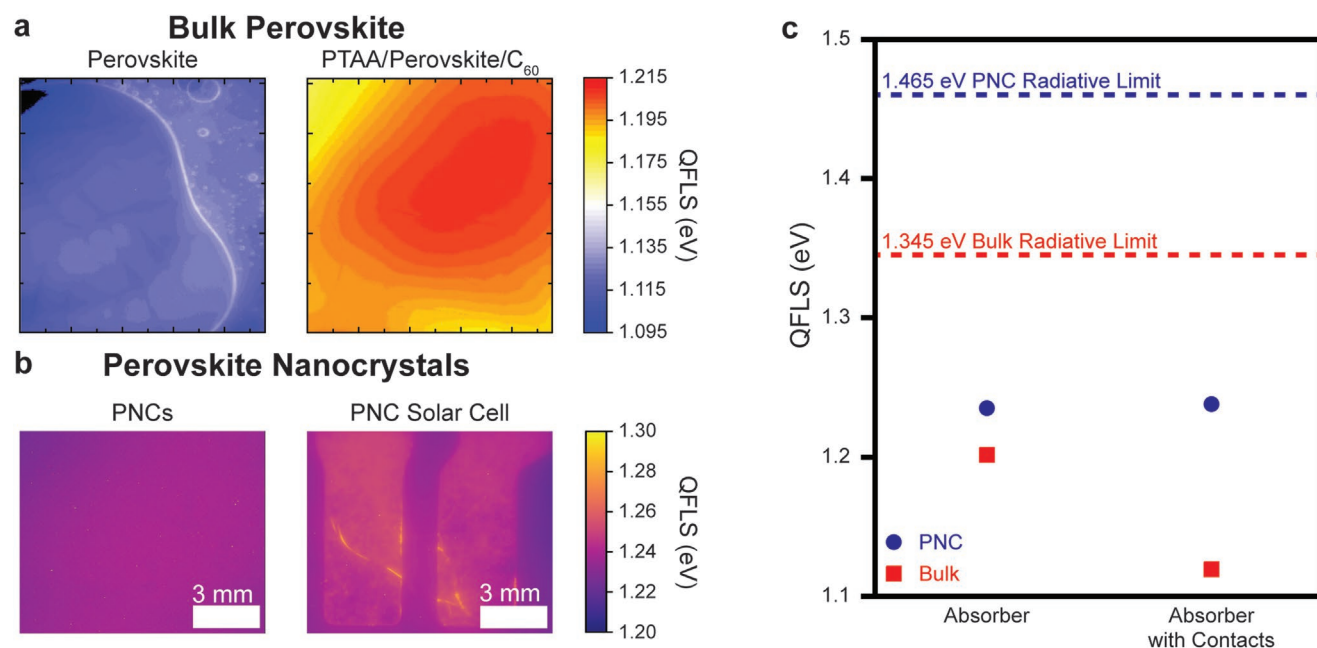


**Figure 5.** QFLS mapping in a) bulk and b) nanocrystalline perovskite films alone or in contact with charge transport layers (in the case of the PNCs, within a full device). c) Comparison of QFLS for bulk and nanocrystal perovskite absorber and absorber with contacts compared to their respective radiative limits. Panel (a) adapted with permission.<sup>[87]</sup> Copyright 2018, Martin Stollerfoht et al. Panel (b) adapted with permission.<sup>[31]</sup> Copyright 2021, American Chemical Society.



charge carriers, especially when the passivation layer is a wide bandgap semiconductor. Case in point, numerous examples have demonstrated improved performance of perovskite solar cells when the 3D bulk MHP is interfaced with a 2D widegap MHP.<sup>[80,113,114]</sup> However, in order not to limit charge extraction, controlling either the relative band alignment or the thickness of the 2D MHP is critical.<sup>[83–85]</sup> In contrast to the 2D/3D MHP heterojunction, PNC-based heterojunctions, as described herein, could be used for similar passivation effects without the limitation to charge extraction caused by the wider bandgaps of 2D perovskites.

Interfaces within PNC solar cells are also responsible for differences in the performance of the *n-i-p* (Figure 6a) versus *p-i-n* (Figure 6b,c) PNC architectures.<sup>[115]</sup> By using Kelvin probe force microscopy (KPFM), electric fields were mapped within CsPbI<sub>3</sub> PNC solar cells. In high-performance *n-i-p* devices, interfaces at both the electron- and hole-transport layers (ETL and HTL; TiO<sub>2</sub> and PTAA, respectively) have strong electric fields (Figure 6a). In *p-i-n* devices, in contrast, the PNC interface with the PTAA HTL has almost no electric field, leading to high interfacial recombination, which limits device performance (Figure 6b). This study also revealed that *p-i-n* PNC solar cells can be improved by synergistically combining PNC and 3D bulk MHP

thin film absorber layers. In this case, the incorporation of a 3D bulk FA<sub>x</sub>MA<sub>1-x</sub>PbI<sub>3</sub> thin film at the HTL/absorber interface dramatically increased the electric field (Figure 6c) and improved *J*<sub>sc</sub> and PCE by nearly an order of magnitude.<sup>[115]</sup> Moreover, the interface between the PNC and thin film MHP shows very little discontinuity in the potential, implying that charge transport is not hindered by the 3D/PNC heterojunction. This concept forms the basis behind the electronic implications of our perspective. Despite the lack of epitaxial connection, charges move unimpeded across PNC/thin film MHP interfaces with similar band positions.

## 6. Passivation of MHP Thin Films using PNCs

Lattice defects at the surface of MHP thin films can be passivated by sequential deposition of PNCs. The addition of Cs<sub>0.05</sub>(MA<sub>0.17</sub>FA<sub>0.83</sub>)<sub>0.95</sub>PbBr<sub>3</sub> PNCs to a (FAPbI<sub>3</sub>)<sub>x</sub>(MAPbBr<sub>3</sub>)<sub>1-x</sub> bulk MHP was found to effectively passivate defects, particularly at grain boundaries.<sup>[44]</sup> Upon annealing, ions from the PNCs were shown to fill atomic vacancies, increasing the *V*<sub>oc</sub> and PCE from 1.02 V and 18.49% (control) to 1.10 V and 20.32% (with PNCs) (Figure 7a,b). Using steady-state and time-resolved

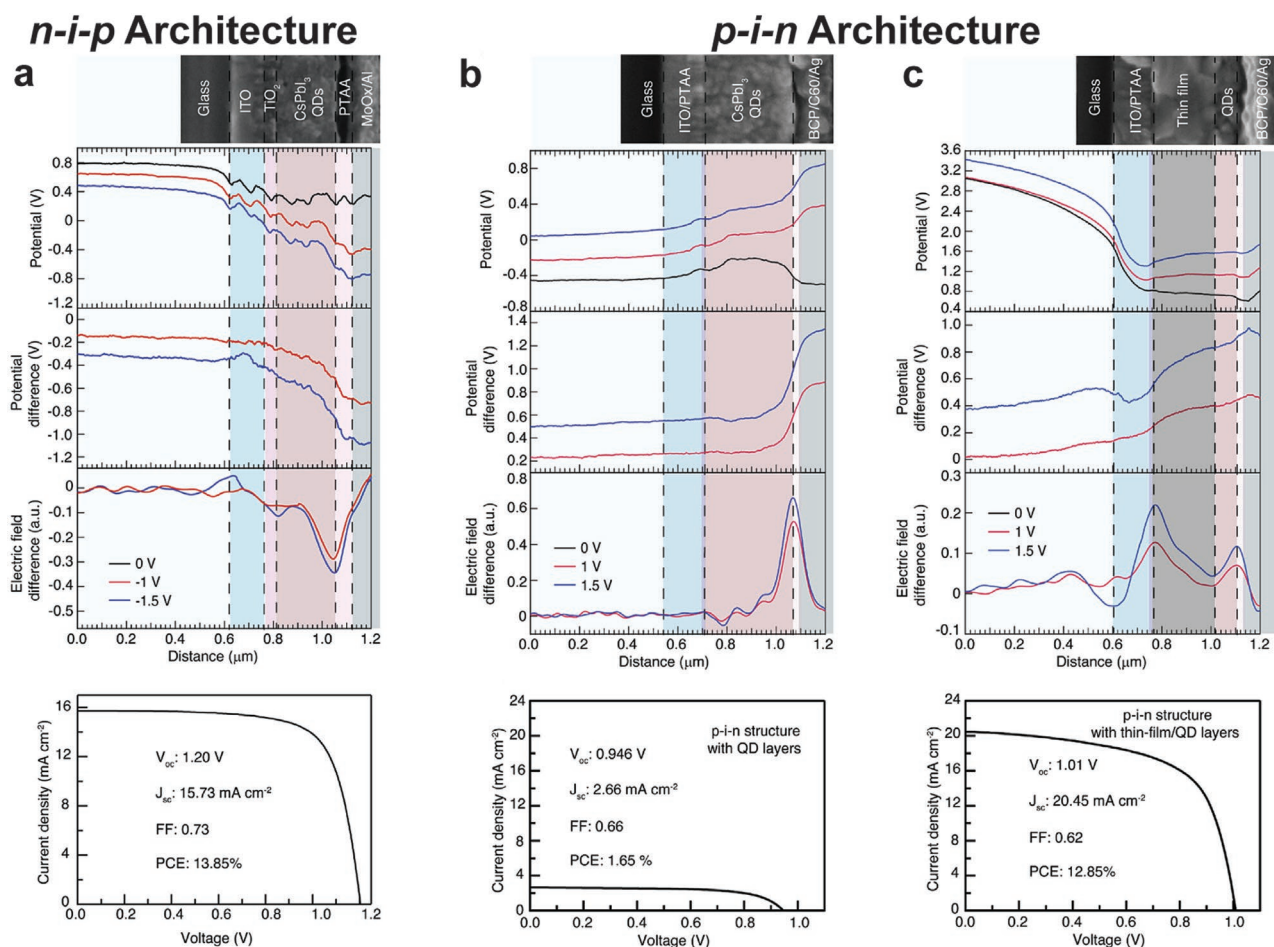


**Figure 6.** KPFM and JV curve measurements for perovskite nanocrystal solar cells in a) *n-i-p* and b,c) *p-i-n* architectures. *p-i-n* devices were fabricated b) without or c) with a perovskite thin film. Adapted with permission.<sup>[115]</sup> Copyright 2020, Elsevier Ltd.

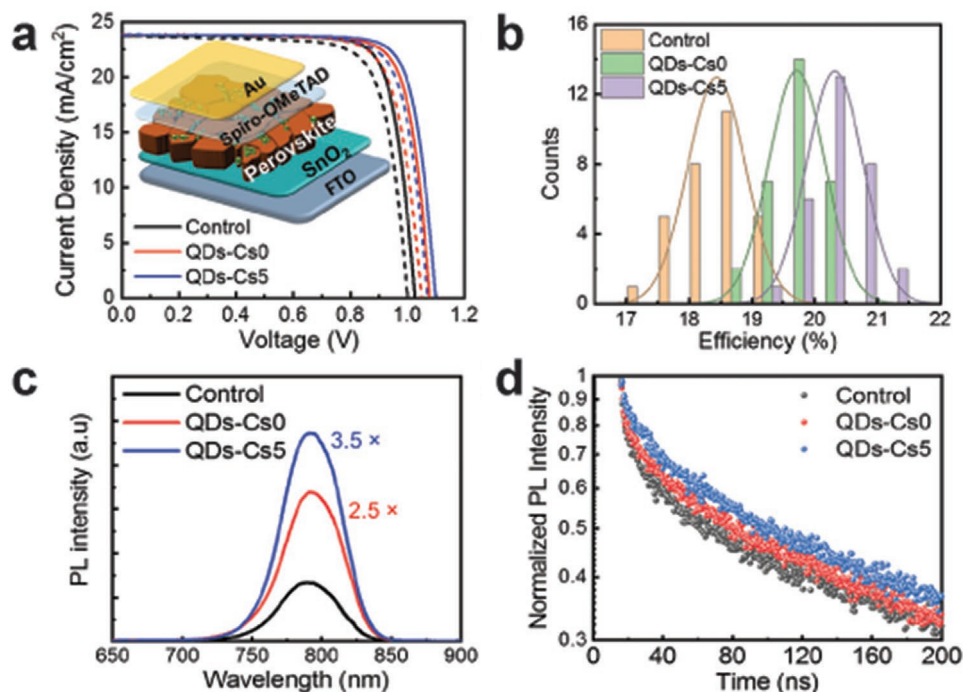


**Figure 7.** a,b) The addition of multi-cation  $\text{Cs}_{0.05}(\text{MA}_{0.17}\text{FA}_{0.83})_{0.95}\text{PbBr}_3$  perovskite nanocrystals significantly improves the performance of  $(\text{FAPbI}_3)_x(\text{MAPbBr}_3)_{1-x}$  bulk perovskite solar cells, particularly as a result of cesium incorporation. c) The photoluminescence intensity was found to increase, as was d) the photoluminescence lifetime, signaling a reduction in defect density and allowing for an improved open circuit voltage. Adapted with permission.<sup>[44]</sup> Copyright 2020, Wiley-VCH GmbH.

photoluminescence (Figure 7c,d) on neat MHP films (without charge transport layers), this treatment was found to reduce non-radiative recombination, increasing the photoluminescence quantum yield from 4.4% to 11.2% and increasing the photoluminescence lifetime. These results indicate that the PNC treatment reduces the defect density within the MHP film, confirmed by thermal admittance spectroscopy experiments that found a reduction in trap density by a factor of ~2.

PNC solutions have also been used to passivate the MHP absorber by acting as a source of both excess ions and surface ligands during antisolvent quenching,<sup>[45,46,116]</sup> as demonstrated by Zheng et al., who used dilute  $\text{CsPbBrCl}_2$  PNC solutions as an antisolvent and passivant for  $\text{MAPbI}_3$  thin film crystallization (Figure 8a,b).<sup>[46]</sup> These passivated  $\text{MAPbI}_3$  solar cells showed reduced band-tail states, smaller trap density, and longer carrier lifetimes, all of which helped to increase  $V_{OC}$ . Unlike other treatment methods, where the PNCs are deposited without dissolution, the PNCs fully dissolve upon contact with the  $\text{MAPbI}_3$  precursor solution in this antisolvent treatment. As a result, the dissolved PNC ions and surface ligands are available for passivation throughout the  $\text{MAPbI}_3$  thin film. Compositional analysis of the film as a function of depth using secondary ion mass spectrometry reveals the presence of elements introduced by the PNCs throughout the entire thickness of the MHP film.

These two studies<sup>[44,46]</sup> point to the importance and difficulty of identifying the root cause for these improvements rather than relying on empirical studies that simply correlate device performance improvements with the presence of additives. In both cases, the primary improvement in solar cell

performance was due to an increase in the  $V_{OC}$ , but there could be several mechanisms responsible for improving the  $V_{OC}$ . PNCs can improve the MHP optoelectronic properties by i) terminating the crystal lattice at either grain boundaries or at the MHP/charge transport layer interface, ii) forming a 3D/2D or 3D/0D interface, iii) providing excess ions to passivate vacancies, or iv) serving as nucleation sites in film formation (when PNCs are introduced prior to crystallization). Several or all of these mechanisms could be responsible for, or at least contribute to, the changes in performance. To understand and tailor future PNC treatments, these mechanisms must be deconvoluted from each other using fundamental characterization rather than simply reporting an improved device performance.

We welcome further scientific understanding of the role of PNCs in benefitting perovskite solar cell performance. Zheng et al. attempted to separate the contributions of ligands and excess ions from PNCs by adding ligands, salts, or both to the antisolvent instead of the PNCs.<sup>[46]</sup> Unfortunately, these control experiments were limited by the insolubility of inorganic salts ( $\text{PbBr}_2$ ,  $\text{PbCl}_2$ ,  $\text{CsBr}$ , or  $\text{CsCl}$ ) in the non-polar toluene antisolvent, which could not be dissolved or dispersed uniformly. Recently reported strategies to deliver these ligands and ions could provide a similar effect as the PNCs by dissolving the salts in a non-polar solvent with the use of amines,<sup>[117]</sup> a strategy that delivers both passivants and excess ions. In this recent study, the use of surface ligands alone did improve PCE, corroborating the beneficial impact of ligand passivation on the  $\text{MAPbI}_3$  film, but the  $V_{OC}$  and PCE did not increase as much as when the PNCs were used.



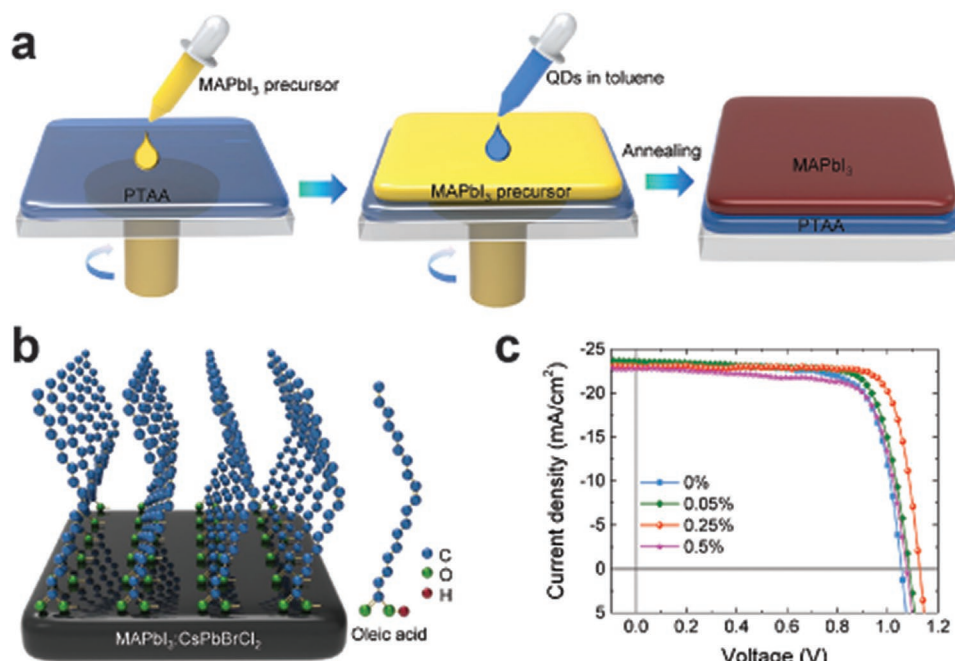


**Figure 8.** a) The addition of perovskite nanocrystals to the MHP thin film during antisolvent quenching b) allows for improved passivation of surfaces and vacancies, c) resulting in improved solar cell performance. Adapted with permission.<sup>[46]</sup> Copyright 2019 Elsevier Inc.

Equally important is understanding the chemical form and morphology of the passivants on the MHP surface, such as determining the protonation of amine or carboxylic acid ligands. Alkyl ammonium ligands from PNCs can form a beneficial 2D/3D interface during MHP film deposition, which has been shown to improve solar cell performance.<sup>[103,118]</sup> In contrast, the appearance of an additional peak in the X-ray diffraction data at low  $2\theta$  reported by Xie et al. suggests that an additional 2D phase forms upon treatment of MHP films with PNCs.<sup>[44]</sup> This 2D/3D interface could increase the photoluminescence quantum yield since similar interfaces are known to reduce non-radiative interfacial charge carrier recombination. Full characterization of the QFLS of the PNC-treated MHP film with or without charge transport layers could help reveal this role.

Lastly, in situ experiments could shed light on the role of PNC inclusions during MHP thin film nucleation, growth, and annealing. Like the recent demonstration of PbS quantum dots embedded in MHP films,<sup>[119–121]</sup> PNCs could act as seed crystals, allowing for efficient nucleation of the bulk MHP film. Unlike PbS quantum dots, PNCs are susceptible to dissolving in the perovskite ink. As a result, the mechanism of this crystallization is likely different and may involve PNC dissolution into MHP precursor colloids, where they could act as crystallization seeds. If this is the case, the colloids may be significantly larger and have more long-range order than the colloids prepared in conventional inks, due to the larger size of the initial PNC inclusions.<sup>[122]</sup> On the other hand, the PNCs might not fully dissolve, allowing direct crystallization of MHP crystallites onto the PNCs. Lastly, the delivery of ligands into the MHP thin film ink might change the crystallization dynamics. Unlike in the case of the PbS QD-seeded growth of MHP thin films,<sup>[119–121]</sup> these PNCs

have long-chain ligands that are insoluble in the polar perovskite ink. Even if the PNC fully dissolves, oleate and oleylammonium ligands (either bound to cesium/lead or bromide/iodide, respectively, or free in solution) could significantly change the local concentration of perovskite precursor ions. These ligands could stabilize small colloidal particles or form micelles within the wet, uncrystallized MHP film, creating a localized increase in the precursor concentration.

## 7. Lower Dimensionality Phases in MHP Heterojunctions

Bandgap tuning through halide selection offers a wide range of bandgaps, but the low activation energy of halide migration ( $\approx 0.6$  eV) ensures rapid compositional homogenization between adjacent MHPs, prohibiting stable perovskite/perovskite heterojunction devices.<sup>[75]</sup> Examples of perovskite/perovskite heterojunctions between dissimilar 3D compositions have therefore been limited. However, in one example a CsPbBr<sub>3</sub>/MAPbCl<sub>3</sub> double-layer LED exhibited nearly double the external quantum efficiency of a single junction CsPbBr<sub>3</sub> LED.<sup>[123]</sup>

In a photovoltaic study, a widegap FAPbBr<sub>3</sub> MHP processed on top of a lower gap triple cation composition established a graded bandgap, enhancing power conversion efficiency by  $\sim 2\%$ .<sup>[124]</sup> One route to improved stability of perovskite/perovskite heterojunctions is modifying the A- or B-site rather than the halide. Sequentially deposited CsPbBr<sub>3</sub>/MASnBr<sub>3</sub> and MAPbBr<sub>3</sub>/MASnBr<sub>3</sub> films, for example, remained heterogeneous after 1500 h, while sequentially deposited films with MA and FA cations mixed in  $< 100$  h, and I<sup>-</sup> and Br<sup>-</sup> mixed in  $< 1$  h.<sup>[125]</sup> Pb<sup>2+</sup> and Sn<sup>2+</sup> were particularly resistant to interdiffusion, with no exchange between films after 60°C heating over 7 h, while

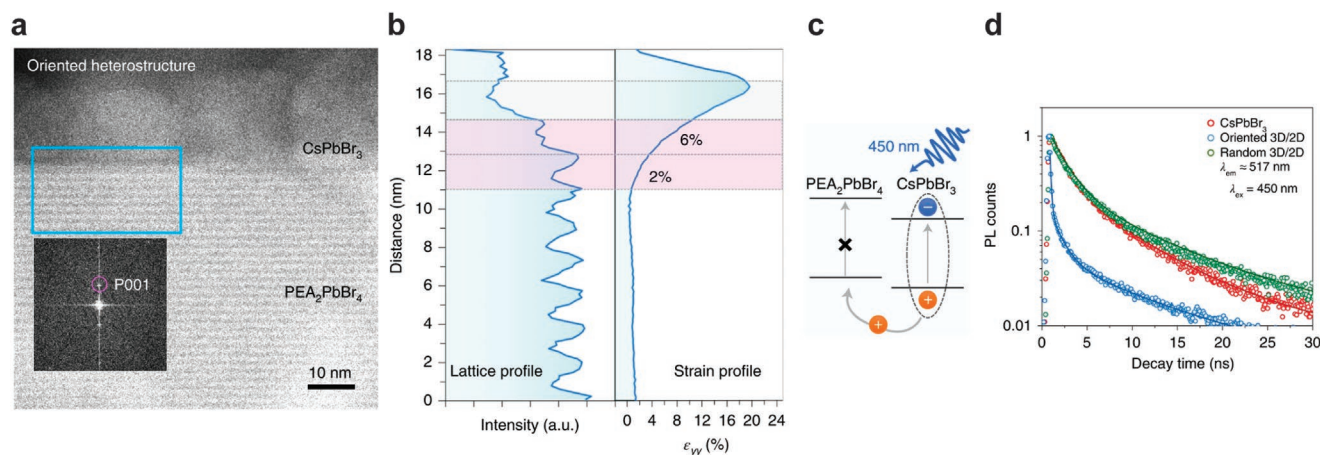


**Figure 9.** Side-view STEM image of a) CsPbBr<sub>3</sub> PNC/2D PEA<sub>2</sub>PbBr<sub>4</sub> and b) the average lattice and strain profile of the region highlighted in the blue rectangle in (a). c) Schematic of charge transfer within the heterostructure under photoexcitation. d) Time-resolved photoluminescence, probed at 517 nm emission wavelength, of CsPbBr<sub>3</sub> PNCs and CsPbBr<sub>3</sub> PNC/2D PEA<sub>2</sub>PbBr<sub>4</sub> heterostructures under 450 nm excitation, demonstrating charge carrier separation when PNCs are oriented with 2D nanoplates. Adapted with permission.<sup>[61]</sup> Copyright 2022, Springer Nature Limited.

MA<sup>+</sup> and FA<sup>+</sup> exchange could be substantially suppressed in films with larger grains.

In contrast to the limited examples of bulk MHP heterojunctions, 2D/3D perovskite heterojunctions have been widely employed since the low diffusivity of the bulky 2D cation ensures the maintenance of discrete interfaces.<sup>[100,102–104,118,126–133]</sup> 2D/3D heterojunctions improve device stability<sup>[100,102,129,131]</sup> as well as device performance through surface passivation<sup>[118,126–132]</sup> or a graded bandgap structure,<sup>[103,133]</sup> and 2D MHPs can also serve as transport layers, replacing metal oxides or organic semiconductors.<sup>[104]</sup> Azmi et al. have demonstrated that 2D/3D MHP interfaces can greatly improve the high-temperature stability of MHP cells, enabling packaged cells to pass 1000-h 85 °C/85% relative humidity exposures.<sup>[102]</sup>

Recently, 2D/PNC heterojunctions have been synthesized through low-temperature welding, resulting in an epitaxial alignment between the 2D and 3D PNC crystal structures.<sup>[61]</sup> High-resolution transmission electron microscopy (TEM) imaging of the interface between CsPbBr<sub>3</sub> PNCs and PEA<sub>2</sub>PbBr<sub>4</sub> (PEA = phenethylammonium) reveals this epitaxial relationship (Figure 9a,b), which is promoted by excess PEA in the 2D phase. These heterostructures result in unique optical properties dependent on the crystallographic fusing of the PNC to the nanoplate (Figure 9c,d). As a result of the type II band offset (Figure 9c), when the PNC is successfully welded to the 2D nanoplate, charge carriers are efficiently separated. This results in a significantly reduced photoluminescence lifetime for oriented 3D/2D heterostructures (Figure 9d). This strategy could be successfully applied to a wide range of applications requiring both charge separation and effective interfacial passivation, taking advantage of the unique properties of both the 2D nanoplate and 3D PNC properties for optoelectronic applications. This strategy could also be applied to the development of heterostructures between PNCs and more conventional bulk 2D semiconductors rather than 2D nanoplates.

Perhaps more on the frontier, lower dimensionality phases like 1D wires and 0D clusters can open new paths toward the use of advantageous quantum confinement as part of the

embodied properties. On this front, we refer readers to a review article on the topic and references therein.<sup>[134]</sup>

## 8. Application of Heterojunctions beyond Photovoltaics

Heterojunctions using PNCs and 2D MHPs are being used in applications beyond photovoltaics. Often, new semiconductor systems are first applied toward existing technology, but new fields of technology can blossom as the field develops and the inherent properties of the new semiconductor can be exploited. MHPs offer plenty of unique properties to be exploited which will lead to new devices that cannot be envisioned yet. Such devices may be enabled by exciting physics from the coupling of organic molecules and inorganic sublattices, the soft nature of the lattice, the strong spin-orbit coupling, strong electron–phonon interactions, and more.

For example, 2D MHP layers constructed with chiral A-sites exhibit a property called chiral-induced spin selectivity (CISS), which permits a spin filtering effect whereby charge carriers are transmitted with specific spin depending on the enantiomer used.<sup>[19,20,24,27,135]</sup> Enantiomers in R- configuration permit transmission of spin-up holes while S- enantiomers facilitate spin-down carrier transport. A chiral 2D CISS layer coupled with PNCs was used to fabricate a room-temperature spin light-emitting diode (LED) shown in Figure 10a.<sup>[24]</sup> The ability to fabricate this CISS/PNC heterojunction benefits from the different solubility of the PNCs and (R-/S-MBA)<sub>2</sub>PbI<sub>4</sub>. As a result of the organic component of the CISS layer, either R- or S-methylbenzylamine (R-/S-MBA), holes are injected into the CsPbI<sub>3</sub> PNC emitter layer with spin preference, resulting in radiative recombination with circularly polarized emission (Figure 10b) controlled by the R-/S- cation. This control of spin, light, and charge could be useful for a wide range of quantum computing and information processing technologies.<sup>[136]</sup>

MHP heterojunctions have also recently been applied to create devices that could enable low-energy information

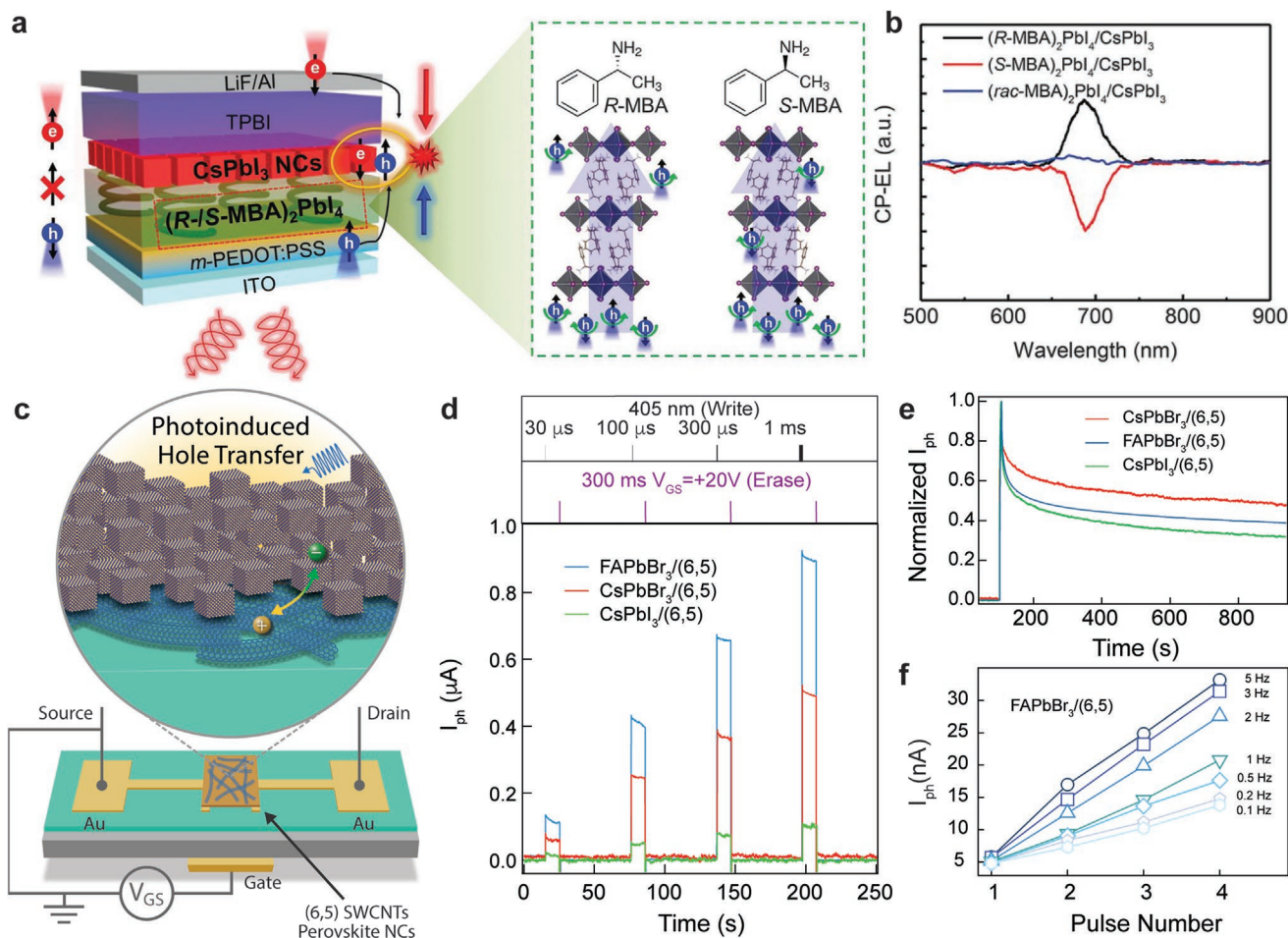


**Figure 10.** a) Schematic illustration of spin-polarized charge injection and CP-EL emission in spin-LEDs. b) CP-EL spectrum of spin-LEDs based on CISS layer/CsPbI<sub>3</sub> NC heterostructure in a.u., arbitrary units. c) Schematic of phototransistor leveraging heterojunction between single-wall carbon nanotubes and perovskite nanocrystals to produce persistent photoconductivity. d) Photoconductivity in single-wall carbon nanotube/perovskite nanocrystal heterojunction during writing (with illumination) and erasing (with applied bias) for multiple compositions of nanocrystals with varying excitation pulse widths. e) Persistent photoconductivity over time in varying compositions of single-wall carbon nanotube/perovskite nanocrystal heterostructures. f) Photocurrent in phototransistor versus pulse number for consecutive pulses at different frequencies. Panels (a) and (b) adapted with permission.<sup>[24]</sup> Copyright 2021, The American Association for the Advancement of Science. Panels (c)–(f) adapted under the terms of the C-CBY license.<sup>[28]</sup> Copyright 2021, the authors, published by Springer Nature.

processing. Persistent photoconductivity is an effect that could be useful for fabricating optical memories and artificial “optical” synapses envisioned for neuromorphic computing and sensing applications. Such persistent photoconductivity can result in MHP-based devices from both charge trapping and/or ion migration. Photo-transistors fabricated with heterostructures of semiconducting single-wall carbon nanotubes (SWCNTs) and PNCs have been shown to exhibit remarkably long-lived persistent photoconductivity (Figure 10c–f) on the order of 1000s of seconds.<sup>[28]</sup> During illumination, holes are transferred to the SWCNTs, electrons are trapped in the PNC layer, and the resulting photoinduced electric field induces halide vacancies to migrate within the MHP layer away from the SWCNT/PNC interface. After the light is turned off, the trapped charges take significant time to equilibrate, leading to exceptionally long (hours) persistent photoconductivity (Figure 10e). Importantly, this photoconductivity can be modulated by both the repetition rate and intensity of the optical excitation and quenched by an

external voltage. This heterojunction can therefore act like an optically driven logic gate. A subsequent study demonstrated that similar heterojunctions formed with PNCs decorated with chiral ligands can enable optical switching that depends on the circular polarization of incident photons.<sup>[137]</sup> In the realm of chirality effects in MHPs, PNCs offer the added advantage of a high surface-to-volume ratio, allowing the surface to be coated with chiral ligands which may not otherwise fit as an A-site molecule within the structure, imparting chirality on the bright emitters.<sup>[137]</sup> Such devices are part of a growing effort to develop circularly polarized light detectors that can efficiently discriminate between right- and left-handed circularly polarized photons and could ultimately enable light-based quantum information processing strategies.<sup>[22,23]</sup>

PNC heterojunctions could bring unique benefits to these emerging types of light-based information processing or lasing devices. For example, graded PNC heterojunctions could potentially lengthen the relaxation time in non-volatile optical



memories. By depositing multiple layers of PNCs with a graded band structure, vacancies and charges can be funneled away from the SWCNT/PNC interface. This may allow even longer-lived optical memory, paving the way to ultra-efficient read/writable memory storage. A circularly polarized detector was recently demonstrated by fabricating an epitaxial heterojunction between a chiral 2D MHP single crystal and its 3D counterpart.<sup>[21]</sup> The large anisotropy factor of the device bodes well for this MHP heterojunction approach, but the low current density is typical of single-crystal devices with large transport lengths that do not rely on a semimetal (such as SWCNTs) for charge transport. A wide variety of chiral PNC layers could be paired with a similarly broad pallet of chiral (or achiral) 2D and 3D MHPs to generate circularly polarized light detectors with broad spectral responses, high responsivities, and large anisotropy ratios.

## 9. Conclusion

Beyond the stand-alone novel properties of MHP semiconductors, new applications will develop based on unique processing and incorporation into complex devices and structures. Heterostructures offer unique ways to synergistically combine different types of MHPs to better control optical, electrical, and structural properties. Orthogonal processing methods, where subsequent layers do not interfere with the underlying layer, are a challenge using traditional MHP deposition techniques. Deposition of nanocrystals is one orthogonal deposition method highlighted here, using nonpolar solution processing through dispersion by their ligands. Heterostructures form the basis of many optoelectronic devices and one recent example to look to for inspiration is the highest efficiency solar cell under 1-sun using quantum well structures to carefully tune the strain and optical properties of III-V semiconductors.<sup>[138]</sup> While MHPs are just establishing the ability to form such structures, devices using III-V materials demonstrate how sophisticated structural control (repeating the quantum well structure hundreds of times) can enable unprecedented performance.

Key to high-performance MHP solar cells is a high degree of control over the charge carriers at the interfaces. Various empirical approaches have demonstrated enormous gains from defect passivation, minority carrier control, and suppression of interfacial recombination losses. Combining this with the insights from PNC-based solar cells that heterojunctions can significantly improve the charge extraction efficiency would suggest that forming heterojunctions between PNCs and 3D or 2D MHPs could offer multiple benefits. Nevertheless, more fundamental studies are needed to clearly elucidate the various effects of ligands and PNC compositions, probing mass transport, epitaxial connection, barrier layers, etc. Further, long-term studies are needed to confirm that such heterostructures can retain their highly beneficial properties against external and activated stresses to operate under real-world conditions without suffering significant losses.

Beyond their use in solar cells, proof-of-principle studies show that PNC-based heterojunctions enable advanced device structures for spintronic and neuromorphic circuits. The groundwork has been laid for systematic studies of innumer-

able possible heterojunctions based on PNCs. We have only just begun to explore how to fabricate and understand the effects imparted by such heterostructures. Beyond the functionality of PNCs in such heterostructures, the processing advantages of PNCs over thin films, as well as their distinct properties, make them an excellent material platform to probe and understand the physics and chemistry of such multilayer constructs on a fundamental level.

## Acknowledgements

This work was authored, in part, by Alliance for Sustainable Energy, LLC, the manager and operator of the National Renewable Energy Laboratory for the U.S. Department of Energy (DOE) under contract no. DE-AC36-08GO28308. The authors acknowledge the Department of Energy Office of Basic Energy Sciences, Office of Science for funding through the Center for Hybrid Organic-Inorganic Semiconductors for Energy (CHOISE), an Energy Frontier Research Center. K.S. and S.N.H. were supported by the director's postdoctoral fellowship program through Laboratory Directed Research and Development at the National Renewable Energy Laboratory.

## Conflict of Interest

The authors declare no conflict of interest.

## Keywords

heterojunctions, nanocrystals, perovskites, photovoltaics, quantum dots

Received: December 22, 2022

Revised: February 14, 2023

Published online: April 25, 2023

- [1] Q. A. Akkerman, L. Manna, *ACS Energy Lett.* **2020**, *5*, 604.
- [2] D. W. Dequillettes, M. Laitz, R. Brenes, B. Dou, B. T. Motes, S. D. Stranks, H. J. Snaith, V. Bulović, D. S. Ginger, *Pure Appl. Chem.* **2020**, *92*, 697.
- [3] Ye Yang, D. P. Ostrowski, R. M. France, K. Zhu, J. Van De Lagemaat, J. M. Luther, M. C. Beard, *Nat. Photonics* **2015**, *10*, 53.
- [4] B. J. Roman, N. M. Villegas, K. Lytle, M. Sheldon, *Nano Lett.* **2020**, *20*, 8874.
- [5] A. F. Palmstrom, G. E. Eperon, T. Leijtens, R. Prasanna, S. N. Habisreutinger, W. Nemeth, E. A. Gaubling, S. P. Dunfield, M. Reese, S. Nanayakkara, T. Moot, J. Werner, J. Liu, B. To, S. T. Christensen, M. D. McGehee, M. F. A. M. Van Hest, J. M. Luther, J. J. Berry, D. T. Moore, *Joule* **2019**, *3*, 2193.
- [6] Z. Li, T. R. Klein, D. H. Kim, M. Yang, J. J. Berry, M. F. A. M. Van Hest, K. Zhu, *Nat. Rev. Mater.* **2018**, *3*, 18017.
- [7] *The Nobel Prize in Physics 2000*, <https://www.nobelprize.org/prizes/physics/2000/summary/>. (accessed April 2023).
- [8] H. Zhong, M. Yang, G. Tang, S. Yuan, *ACS Energy Lett.* **2020**, *5*, 2275.
- [9] Z. Nie, X. Gao, Y. Ren, S. Xia, Y. Wang, Y. Shi, J. Zhao, Y. Wang, *Nano Lett.* **2020**, *20*, 4610.
- [10] S. Kaniyankandy, S. Neogy, *J. Photochem. Photobiol., A* **2020**, *401*, 112761.
- [11] X. Wu, M. T. Trinh, D. Niesner, H. Zhu, Z. Norman, J. S. Owen, O. Yaffe, B. J. Kudisch, X.-Y. Zhu, *J. Am. Chem. Soc.* **2015**, *137*, 2089.

- [12] Y. Zhai, S. Baniya, C. Zhang, J. Li, P. Haney, C.-X. Sheng, E. Ehrenfreund, Z. V. Vardeny, *Sci. Adv.* **2017**, *3*, 1700704.
- [13] D. Giovanni, W. K. Chong, H. A. Dewi, K. Thirumal, I. Neogi, R. Ramesh, S. Mhaisalkar, N. Mathews, T. C. Sum, *Sci. Adv.* **2016**, *2*, 1600477.
- [14] C. Zhang, D. Sun, C.-X. Sheng, Y. X. Zhai, K. Mielczarek, A. Zakhidov, Z. V. Vardeny, *Nat. Phys.* **2015**, *11*, 427.
- [15] Y.-C. Hsiao, T. Wu, M. Li, B. Hu, *Adv. Mater.* **2015**, *27*, 2899.
- [16] Z. G. Yu, *Sci. Rep.* **2016**, *6*, 28576.
- [17] M. Kepenekian, R. Robles, C. Katan, D. Saponi, L. Pedesseau, J. Even, *ACS Nano* **2015**, *9*, 11557.
- [18] Y. -H. Kim, Y. Zhai, E. A. Gaubling, S. N. Habisreutinger, T. Moot, B. A. Rosales, H. Lu, A. Hazarika, R. Brunecky, L. M. Wheeler, J. J. Berry, M. C. Beard, J. M. Luther, *ACS Nano* **2020**, *14*, 8816.
- [19] J. Wang, H. Lu, X. Pan, J. Xu, H. Liu, X. Liu, D. R. Khanal, M. F. Toney, M. C. Beard, Z. V. Vardeny, *ACS Nano* **2021**, *15*, 588.
- [20] H. Lu, C. Xiao, R. Song, T. Li, A. E. Maughan, A. Levin, R. Brunecky, J. J. Berry, D. B. Mitzi, V. Blum, M. C. Beard, *J. Am. Chem. Soc.* **2020**, *142*, 13030.
- [21] X. Zhang, X. Liu, L. Li, C. Ji, Y. Yao, J. Luo, *ACS Cent. Sci.* **2021**, *7*, 1261.
- [22] X. Shang, Li Wan, L. Wang, F. Gao, H. Li, *J. Mater. Chem. C* **2022**, *10*, 2400.
- [23] Ji Hao, H. Lu, L. Mao, X. Chen, M. C. Beard, J. L. Blackburn, *ACS Nano* **2021**, *15*, 7608.
- [24] Y.-H. Kim, Y. Zhai, H. Lu, X. Pan, C. Xiao, E. A. Gaubling, S. P. Harvey, J. J. Berry, Z. V. Vardeny, J. M. Luther, M. C. Beard, *Science* **2021**, *371*, 1129.
- [25] M. J. Crane, L. M. Jacoby, T. A. Cohen, Y. Huang, C. K. Luscombe, D. R. Gamelin, *Nano Lett.* **2020**, *20*, 8626.
- [26] T. Qiao, X. Liu, D. Rossi, M. Khurana, Y. Lin, J. Wen, J. Cheon, A. V. Akimov, D. H. Son, *Nano Lett.* **2021**, *21*, 9543.
- [27] H. Lu, J. Wang, C. Xiao, X. Pan, X. Chen, R. Brunecky, J. J. Berry, K. Zhu, M. C. Beard, Z. V. Vardeny, *Sci. Adv.* **2019**, *5*, aay0571.
- [28] Ji Hao, Y.-H. Kim, S. N. Habisreutinger, S. P. Harvey, E. M. Miller, S. M. Foradori, M. S. Arnold, Z. Song, Y. Yan, J. M. Luther, J. L. Blackburn, *Sci. Adv.* **2021**, *7*, abf1959.
- [29] K. Sakhatskyi, R. A. John, A. Guerrero, S. Tsarev, S. Sabisch, T. Das, G. J. Matt, S. Yakunin, I. Cherniukh, M. Kotyrba, Y. Berezovska, M. I. Bodnarchuk, S. Chakraborty, J. Bisquert, M. V. Kovalenko, *ACS Energy Lett.* **2022**, *7*, 3401.
- [30] W. Tress, *J. Phys. Chem. Lett.* **2017**, *8*, 3106.
- [31] B. M. Wieliczka, J. A. Márquez, A. M. Bothwell, Q. Zhao, T. Moot, K. T. Vansant, A. J. Ferguson, T. Unold, D. Kuciauskas, J. M. Luther, *ACS Nano* **2021**, *15*, 19334.
- [32] F. Di Stasio, S. Christodoulou, N. Huo, G. Konstantatos, *Chem. Mater.* **2017**, *29*, 7663.
- [33] A. Dutta, R. K. Behera, P. Pal, S. Baitalik, N. Pradhan, *Angew. Chem., Int. Ed.* **2019**, *58*, 5552.
- [34] J. Pan, Y. Shang, J. Yin, M. De Bastiani, W. Peng, I. Dursun, L. Sinatra, A. M. El-Zohry, M. N. Hedhili, A. -H. Emwas, O. F. Mohammed, Z. Ning, O. M. Bakr, *J. Am. Chem. Soc.* **2018**, *140*, 562.
- [35] B. A. Koscher, J. K. Swabeck, N. D. Bronstein, A. P. Alivisatos, *J. Am. Chem. Soc.* **2017**, *139*, 6566.
- [36] D. P. Nenon, K. Pressler, J. Kang, B. A. Koscher, J. H. Olshansky, W. T. Osowiecki, M. A. Koc, L.-W. Wang, A. P. Alivisatos, *J. Am. Chem. Soc.* **2018**, *140*, 17760.
- [37] A. Hazarika, Q. Zhao, E. A. Gaubling, J. A. Christians, B. Dou, A. R. Marshall, T. Moot, J. J. Berry, J. C. Johnson, J. M. Luther, *ACS Nano* **2018**, *12*, 10327.
- [38] L. Protesescu, S. Yakunin, M. I. Bodnarchuk, F. Krieg, R. Caputo, C. H. Hendon, R. Xi Yang, A. Walsh, M. V. Kovalenko, *Nano Lett.* **2015**, *15*, 3692.
- [39] L. Protesescu, S. Yakunin, S. Kumar, J. Bär, F. Bertolotti, N. Masciocchi, A. Guagliardi, M. Grotevent, I. Shorubalko, M. I. Bodnarchuk, C.-J. Shih, M. V. Kovalenko, *ACS Nano* **2017**, *11*, 3119.
- [40] I. Lignos, V. Morad, Y. Shynkarenko, C. Bernasconi, R. M. Maceiczky, L. Protesescu, F. Bertolotti, S. Kumar, S. T. Ochsenbein, N. Masciocchi, A. Guagliardi, C.-J. Shih, M. I. Bodnarchuk, A. J. Demello, M. V. Kovalenko, *ACS Nano* **2018**, *12*, 5504.
- [41] I. Levchuk, A. Osvet, X. Tang, M. Brandl, J. D. Perea, F. Hoegl, G. J. Matt, R. Hock, M. Batentschuk, C. J. Brabec, *Nano Lett.* **2017**, *17*, 2765.
- [42] F. Zhang, H. Zhong, C. Chen, X.-G. Wu, X. Hu, H. Huang, J. Han, B. Zou, Y. Dong, *ACS Nano* **2015**, *9*, 4533.
- [43] R. W. Epps, M. S. Bowen, A. A. Volk, K. Abdel-Latif, S. Han, K. G. Reyes, A. Amassian, M. Abolhasani, *Adv. Mater.* **2020**, *32*, 2001626.
- [44] L. Xie, P. Vashishtha, T. M. Koh, P. C. Harikesh, N. F. Jamaludin, A. Bruno, T. J. N. Hooper, J. Li, Y. F. Ng, S. G. Mhaisalkar, N. Mathews, *Adv. Mater.* **2020**, *32*, 2003296.
- [45] M. Que, Z. Dai, H. Yang, H. Zhu, Y. Zong, W. Que, N. P. Padture, Y. Zhou, Ou Chen, *ACS Energy Lett.* **2019**, *4*, 1970.
- [46] X. Zheng, J. Troughton, N. Gasparini, Y. Lin, M. Wei, Yi Hou, J. Liu, K. Song, Z. Chen, C. Yang, B. Turedi, A. Y. Alsalloum, J. Pan, J. Chen, A. A. Zhumekenov, T. D. Anthopoulos, Yu Han, D. Baran, O. F. Mohammed, E. H. Sargent, O. M. Bakr, *Joule* **2019**, *3*, 1963.
- [47] C. Hanmandlu, S. Swamy, A. Singh, Hsin-An Chen, C.-C. Liu, C.-S. Lai, A. Mohapatra, C.-W. Pao, P. Chen, C.-W. Chu, *J. Mater. Chem. A* **2020**, *8*, 5263.
- [48] Q. Zhao, A. Hazarika, L. T. Schelhas, J. Liu, E. A. Gaubling, G. Li, M. Zhang, M. F. Toney, P. C. Sercel, J. M. Luther, *ACS Energy Lett.* **2020**, *5*, 238.
- [49] C.-H. Lu, G. V. Biesold-Mcgee, Y. Liu, Z. Kang, Z. Lin, *Chem. Soc. Rev.* **2020**, *49*, 4953.
- [50] Q. Zhao, A. Hazarika, X. Chen, S. P. Harvey, B. W. Larson, G. R. Teeter, J. Liu, T. Song, C. Xiao, L. Shaw, M. Zhang, G. Li, M. C. Beard, J. M. Luther, *Nat. Commun.* **2019**, *10*, 2842.
- [51] X. Ling, S. Zhou, J. Yuan, J. Shi, Y. Qian, B. W. Larson, Q. Zhao, C. Qin, F. Li, G. Shi, C. Stewart, J. Hu, X. Zhang, J. M. Luther, S. Duhm, W. Ma, *Adv. Energy Mater.* **2019**, *9*, 1900721.
- [52] M. Suri, A. Hazarika, B. W. Larson, Q. Zhao, M. Vallés-Pelarda, T. D. Siegler, M. K. Abney, A. J. Ferguson, B. A. Korgel, J. M. Luther, *ACS Energy Lett.* **2019**, *4*, 1954.
- [53] Y. Wang, J. Yuan, X. Zhang, X. Ling, B. W. Larson, Q. Zhao, Y. Yang, Y. Shi, J. M. Luther, W. Ma, *Adv. Mater.* **2020**, *32*, 2000449.
- [54] E. M. Sanehira, A. R. Marshall, J. A. Christians, S. P. Harvey, P. N. Ciesielski, L. M. Wheeler, P. Schulz, L. Y. Lin, M. C. Beard, J. M. Luther, *Sci. Adv.* **2017**, *3*, aao4204.
- [55] D. Jia, J. Chen, M. Yu, J. Liu, E. M. J. Johansson, A. Hagfeldt, X. Zhang, *Small* **2020**, *16*, 2001772.
- [56] X. Ling, J. Yuan, X. Zhang, Y. Qian, S. M. Zakeeruddin, B. W. Larson, Q. Zhao, J. Shi, J. Yang, K. Ji, Y. Zhang, Y. Wang, C. Zhang, S. Duhm, J. M. Luther, M. Grätzel, W. Ma, *Adv. Mater.* **2020**, *32*, 2001906.
- [57] Y. Liu, Y. Dong, T. Zhu, D. Ma, A. Proppe, B. Chen, C. Zheng, Yi Hou, S. Lee, B. Sun, E. H. Jung, F. Yuan, Ya-K Wang, L. K. Sagar, S. Hoogland, F. P. García De Arquer, M.-J. Choi, K. Singh, S. O. Kelley, O. Voznyy, Z.-H. Lu, E. H. Sargent, *J. Am. Chem. Soc.* **2021**, *143*, 15606.
- [58] S. Y. Park, H. C. Shim, *ACS Appl. Mater. Interfaces* **2020**, *12*, 57124.
- [59] H. Bian, D. Bai, Z. Jin, K. Wang, L. Liang, H. Wang, J. Zhang, Q. Wang, S. F. Liu, *Joule* **2018**, *2*, 1500.
- [60] F. Li, S. Zhou, J. Yuan, C. Qin, Y. Yang, J. Shi, X. Ling, Y. Li, W. Ma, *ACS Energy Lett.* **2019**, *4*, 2571.

- [61] Z. Zhu, C. Zhu, L. Yang, Q. Chen, L. Zhang, J. Dai, J. Cao, S. Zeng, Z. Wang, Z. Wang, W. Zhang, J. Bao, L. Yang, Y. Yang, Bo Chen, C. Yin, H. Chen, Y. Cao, H. Gu, J. Yan, N. Wang, G. Xing, H. Li, X. Wang, S. Li, Z. Liu, H. Zhang, L. Wang, X. Huang, W. Huang, *Nat. Mater.* **2022**, 21, 1042.
- [62] Z. Zhou, H. W. Qiao, Y. Hou, H. G. Yang, S. Yang, *Energy Environ. Sci.* **2021**, 14, 127.
- [63] E. Shi, L. Dou, *Acc Mater Res* **2020**, 1, 213.
- [64] R. Su, Z. Xu, J. Wu, D. Luo, Q. Hu, W. Yang, X. Yang, R. Zhang, H. Yu, T. P. Russell, Q. Gong, W. Zhang, R. Zhu, *Nat. Commun.* **2021**, 12, 2479.
- [65] He Huang, M. I. Bodnarchuk, S. V. Kershaw, M. V. Kovalenko, A. L. Rogach, *ACS Energy Lett.* **2017**, 2, 2071.
- [66] K. X. Steirer, P. Schulz, G. Teeter, V. Stevanovic, M. Yang, K. Zhu, J. J. Berry, *ACS Energy Lett.* **2016**, 1, 360.
- [67] M. Wang, C. Fei, Md. A Uddin, J. Huang, *Sci. Adv.* **2022**, 8, abo5977.
- [68] Q. A. Akkerman, T. P. T. Nguyen, S. C. Boehme, F. Montanarella, D. N. Dirin, P. Wechsler, F. Beiglböck, G. Rainò, R. Erni, C. Katan, J. Even, M. V. Kovalenko, *Science* **2022**, 377, 1406.
- [69] M. P. Hautzinger, E. K. Raulerson, S. P. Harvey, T. Liu, D. Duke, X. Qin, R. A. Scheidt, B. M. Wieliczka, A. J. Phillips, K. R. Graham, V. Blum, J. M. Luther, M. C. Beard, J. L. Blackburn, *J. Am. Chem. Soc.* **2023**, 145, 2052.
- [70] D. B. Sulas-Kern, E. M. Miller, J. L. Blackburn, *Energy Environ. Sci.* **2020**, 13, 2684.
- [71] E. M. Miller, Y. Zhao, C. C. Mercado, S. K. Saha, J. M. Luther, K. Zhu, V. Stevanović, C. L. Perkins, J. Van De Lagemaat, *Phys. Chem. Chem. Phys.* **2014**, 16, 22122.
- [72] P. Schulz, A.-M. Dowgiallo, M. Yang, K. Zhu, J. L. Blackburn, J. J. Berry, *J. Phys. Chem. Lett.* **2016**, 7, 418.
- [73] E. Amerling, Y. Zhai, B. W. Larson, Yi Yao, B. Fluegel, Z. Owczarczyk, H. Lu, L. Whittaker-Brooks, V. Blum, J. L. Blackburn, *J. Mater. Chem. A* **2021**, 9, 14977.
- [74] Z. Chen, Y. Liu, S. Gong, Z. Zhang, Q. Cao, L. Mao, X. Chen, H. Lu, *J. Chem. Phys.* **2022**, 157, 084705.
- [75] T. Elmelund, R. A. Scheidt, B. Seger, P. V. Kamat, *ACS Energy Lett.* **2019**, 4, 1961.
- [76] Y.-W. Jang, S. Lee, K. M. Yeom, K. Jeong, K. Choi, M. Choi, J. H. Noh, *Nat. Energy* **2021**, 6, 63.
- [77] P. Guo, Da Liu, X. Shen, Q. Lv, Yu Wu, Q. Yang, Pu Li, Y. Hao, J. C. Ho, K. M. Yu, *Nano Energy* **2022**, 92, 106778.
- [78] D. Lin, T. Zhang, J. Wang, M. Long, F. Xie, J. Chen, B. Wu, T. Shi, K. Yan, W. Xie, P. Liu, J. Xu, *Nano Energy* **2019**, 59, 619.
- [79] R. Azmi, E. Ugur, A. Seitkhan, F. Aljamaan, A. S. Subbiah, J. Liu, G. T. Harrison, M. I. Nugraha, M. K. Eswaran, M. Babics, Y. Chen, F. Xu, T. G. Allen, A. Ur Rehman, C.-L. Wang, T. D. Anthopoulos, U. Schwingenschlögl, M. De Bastiani, E. Aydin, S. De Wolf, *Science* **2022**, 376, 73.
- [80] G. Wu, R. Liang, M. Ge, G. Sun, Y. Zhang, G. Xing, *Adv. Mater.* **2022**, 34, 2105635.
- [81] Q. He, M. Worku, L. Xu, C. Zhou, H. Lin, A. J. Robb, K. Hanson, Y. Xin, B. Ma, *ACS Appl. Mater. Interfaces* **2020**, 12, 1159.
- [82] E-Bi Kim, M. S Akhtar, H.-S. Shin, S. Ameen, M. K. Nazeeruddin, *J. Photochem. Photobiol., C* **2021**, 48, 100405.
- [83] J. J. Yoo, G. Seo, M. R. Chua, T. G. Park, Y. Lu, F. Rotermund, Y.-K. Kim, C. Su Moon, N. J. Jeon, J.-P. Correa-Baena, V. Bulović, S. S. Shin, M. G. Bawendi, J. Seo, *Nature* **2021**, 590, 587.
- [84] H. Min, D. Y Lee, J. Kim, G. Kim, K. S. Lee, J. Kim, M. J. Paik, Y. Ki Kim, K. S. Kim, M. G. Kim, T. J. Shin, S. Il Seok, *Nature* **2021**, 598, 444.
- [85] H. Chen, S. Teale, B. Chen, Yi Hou, L. Grater, T. Zhu, K. Bertens, S. M Park, H. R. Atapattu, Y. Gao, M. Wei, A. K. Johnston, Q. Zhou, K. Xu, D. Yu, C. Han, T. Cui, E. H. Jung, C. Zhou, W. Zhou, A. H. Proppe, S. Hoogland, F. Laquai, T. Filleter, K. R. Graham, Z. Ning, E. H. Sargent, *Nat. Photonics* **2022**, 16, 352.
- [86] L. M. Wheeler, E. M. Sanehira, A. R. Marshall, P. Schulz, M. Suri, N. C. Anderson, J. A. Christians, D. Nordlund, D. Sokaras, T. Kroll, S. P. Harvey, J. J. Berry, L. Y. Lin, J. M. Luther, *J. Am. Chem. Soc.* **2018**, 140, 10504.
- [87] M. Stolterfoht, C. M. Wolff, J. A. Márquez, S. Zhang, C. J. Hages, D. Rothhardt, S. Albrecht, P. L. Burn, P. Meredith, T. Unold, D. Neher, *Nat. Energy* **2018**, 3, 847.
- [88] K. Schutt, R. Kerner, A. Maughan, A. Palmstrom, S. Habisreutinger, J. Berry, *Halide Organic Photovoltaics for Energy: Hybrid Perovskites for Solar Cells.*, [https://doi.org/10.1142/9789811242076\\_0001](https://doi.org/10.1142/9789811242076_0001).
- [89] A. Kojima, K. Teshima, Y. Shirai, T. Miyasaka, *J. Am. Chem. Soc.* **2009**, 131, 6050.
- [90] Z. Li, M. Yang, Ji-S Park, Su-H Wei, J. J. Berry, K. Zhu, **2016**, 28, 284.
- [91] J. Xu, C. C. Boyd, Z. J. Yu, A. F. Palmstrom, D. J. Witter, B. W. Larson, R. M. France, J. Werner, S. P. Harvey, E. J. Wolf, W. Weigand, S. Manzoor, M. F. A. M. Van Hest, J. J. Berry, J. M. Luther, Z. C. Holman, M. D. McGehee, *Science* **2020**, 367, 1097.
- [92] J.-W. Lee, H.-S. Kim, N.-G. Park, *Acc. Chem. Res.* **2016**, 49, 311.
- [93] D. N. Dirin, I. Cherniukh, S. Yakunin, Y. Shynkarenko, M. V. Kovalenko, *Chem. Mater.* **2016**, 28, 8470.
- [94] Y. Liu, Z. Yang, D. Cui, X. Ren, J. Sun, X. Liu, J. Zhang, Q. Wei, H. Fan, F. Yu, Xu Zhang, C. Zhao, S. F. Liu, *Adv. Mater.* **2015**, 27, 5176.
- [95] M. C. Weidman, M. Seitz, S. D. Stranks, W. A. Tisdale, *ACS Nano* **2016**, 10, 7830.
- [96] D. Zhang, Yi Yu, Y. Bekenstein, A. B. Wong, A. P. Alivisatos, P. Yang, *J. Am. Chem. Soc.* **2016**, 138, 13155.
- [97] P. Gui, H. Zhou, F. Yao, Z. Song, B. Li, G. Fang, *Small* **2019**, 15, 1902618.
- [98] D. Zhang, S. W. Eaton, Yi Yu, L. Dou, P. Yang, *J. Am. Chem. Soc.* **2015**, 137, 9230.
- [99] Y. Dong, T. Qiao, D. Kim, D. Parobek, D. Rossi, D. H. Son, *Nano Lett.* **2018**, 18, 3716.
- [100] G. Grancini, C. Roldán-Carmona, I. Zimmermann, E. Mosconi, X. Lee, D. Martineau, S. Narbey, F. Oswald, F. De Angelis, M. Graetzel, M. K. Nazeeruddin, *Nat. Commun.* **2017**, 8, 15684.
- [101] K.-H. Wang, L. Wu, L. Li, H.-B. Yao, H.-S. Qian, S.-H. Yu, *Angew. Chem., Int. Ed.* **2016**, 55, 8328.
- [102] R. Azmi, E. Ugur, A. Seitkhan, F. Aljamaan, A. S. Subbiah, J. Liu, G. T. Harrison, M. I. Nugraha, M. K. Eswaran, M. Babics, Y. Chen, F. Xu, T. G. Allen, A. U. Rehman, C.-L. Wang, T. D. Anthopoulos, U. Schwingenschlögl, M. De Bastiani, E. Aydin, S. De Wolf, *Science* **2022**, 376, 73.
- [103] S. Jeong, S. Seo, H. Yang, H. Park, S. Shin, H. Ahn, D. Lee, J. H. Park, N.-G. Park, H. Shin, *Adv. Energy Mater.* **2021**, 11, 2102236.
- [104] T. Zhang, M. Long, M. Qin, X. Lu, Si Chen, F. Xie, Li Gong, J. Chen, M. Chu, Q. Miao, Z. Chen, W. Xu, P. Liu, W. Xie, J.-B. Xu, *Joule* **2018**, 2, 2706.
- [105] A. Rajagopal, R. J. Stoddard, S. B. Jo, H. W. Hillhouse, A. K.-Y. Jen, *Nano Lett.* **2018**, 18, 3985.
- [106] M. Yang, T. Zhang, P. Schulz, Z. Li, Ge Li, D. H. Kim, N. Guo, J. J. Berry, K. Zhu, Y. Zhao, *Nat. Commun.* **2016**, 7, 12305.
- [107] J. Jeong, M. Kim, J. Seo, H. Lu, P. Ahlawat, A. Mishra, Y. Yang, M. A. Hope, F. T. Eickemeyer, M. Kim, Y. J. Yoon, I. W. Choi, B. P. Darwich, S. J. Choi, Y. Jo, J. H. Lee, B. Walker, S. M. Zakeeruddin, L. Emsley, U. Rothlisberger, A. Hagfeldt, D. S. Kim, M. Grätzel, J. Y. Kim, *Nature* **2021**, 592, 381.
- [108] Y. Li, H. Xie, E. L. Lim, A. Hagfeldt, D. Bi, *Adv. Energy Mater.* **2021**, 12, 2102730.
- [109] I. L. Braly, D. W. Dequillettes, L. M. Pazos-Outón, S. Burke, M. E. Ziffer, D. S. Ginger, H. W. Hillhouse, *Nat. Photonics* **2018**, 12, 355.
- [110] S. Jariwala, S. Burke, S. Dunfield, R. C. Shallcross, M. Taddei, J. Wang, G. E. Eperon, N. R. Armstrong, J. J. Berry, D. S. Ginger, *Chem. Mater.* **2021**, 33, 5035.



- [111] W.-J. Yin, T. Shi, Y. Yan, *Appl. Phys. Lett.* **2014**, *104*, 063903.
- [112] J. Warby, F. Zu, S. Zeiske, E. Gutierrez-Partida, L. Frohloff, S. Kahmann, K. Frohna, E. Mosconi, E. Radicchi, F. Lang, S. Shah, F. Peña-Camargo, H. Hempel, T. Unold, N. Koch, A. Armin, F. De Angelis, S. D. Stranks, D. Neher, M. Stolterfoht, *Adv. Energy Mater.* **2022**, *12*, 2103567.
- [113] S. Sidhik, Y. Wang, M. De Siena, R. Asadpour, A. J. Torma, T. Terlier, K. Ho, W. Li, A. B. Puthirath, X. Shuai, A. Agrawal, B. Traore, M. Jones, R. Giridharagopal, P. M. Ajayan, J. Strzalka, D. S. Ginger, C. Katan, M. A. Alam, J. Even, M. G. Kanatzidis, A. D. Mohite, *Science* **2022**, *377*, 1425.
- [114] J. Y. Ye, J. Tong, J. Hu, C. Xiao, H. Lu, S. P. Dunfield, D. H. Kim, X. Chen, B. W. Larson, Ji Hao, K. Wang, Q. Zhao, Z. Chen, H. Hu, W. You, J. J. Berry, F. Zhang, K. Zhu, *Sol. RRL* **2020**, *4*, 2000082.
- [115] C. Xiao, Q. Zhao, C.-S. Jiang, Y. Sun, M. M. Al-Jassim, S. U. Nanayakkara, J. M. Luther, *Nano Energy* **2020**, *78*, 105319.
- [116] Y. Chen, Y. Zhao, *J. Mater. Chem. A* **2020**, *8*, 25017.
- [117] N. K. Noel, B. Wenger, S. N. Habisreutinger, H. J. Snaith, *ACS Energy Lett.* **2022**, *7*, 1246.
- [118] M. A. Mahmud, T. Duong, Y. Yin, H. T. Pham, D. Walter, J. Peng, Y. Wu, Li Li, H. Shen, N. Wu, N. Mozaffari, G. Andersson, K. R. Catchpole, K. J. Weber, T. P. White, *Adv. Funct. Mater.* **2019**, *30*, 1907962.
- [119] S.-S. Li, C.-H. Chang, Y.-C. Wang, C. Lin, D.-Y. Wang, J.-C. Lin, C.-C. Chen, H.-S. Sheu, H.-C. Chia, W.-R. Wu, U.-S. Jeng, C.-T. Liang, R. Sankar, F.-C. Chou, C.-W. Chen, *Energy Environ. Sci.* **2016**, *9*, 1282.
- [120] C.-Y. Lin, S.-S. Li, J.-W. Chang, H.-C. Chia, Y.-Y. Hsiao, C.-J. Su, B.-J. Lian, C.-Y. Wen, S.-K. Huang, W.-R. Wu, D.-Y. Wang, A.-C. Su, C.-W. Chen, U.-S. Jeng, *Adv. Funct. Mater.* **2019**, *29*, 1902582.
- [121] S. Masi, C. Echeverría-Arrondo, K. M. M. Salim, T. T. Ngo, P. F. Mendez, E. López-Fraguas, D. F. Macias-Pinilla, J. Planelles, J. I. Climente, I. Mora-Seró, *ACS Energy Lett.* **2020**, *5*, 418.
- [122] N. S. Dutta, N. K. Noel, C. B. Arnold, *J. Phys. Chem. Lett.* **2020**, *11*, 5980.
- [123] D.-H. Kang, S.-G. Kim, Y. C. Kim, I. T. Han, H. J. Jang, J. Y. Lee, N.-G. Park, *ACS Energy Lett.* **2020**, *5*, 2191.
- [124] K. T. Cho, S. Paek, G. Grancini, C. Roldán-Carmona, P. Gao, Y. Lee, M. K. Nazeeruddin, *Energy Environ. Sci.* **2017**, *10*, 621.
- [125] C. P. Clark, J. E. Mann, J. S. Bangsund, W.-Ju Hsu, E. S. Aydil, R. J. Holmes, *ACS Energy Lett.* **2020**, *5*, 3443.
- [126] D. Luo, W. Yang, Z. Wang, A. Sadhanala, Q. Hu, R. Su, R. Shivanna, G. F. Trindade, J. F. Watts, Z. Xu, T. Liu, Ke Chen, F. Ye, P. Wu, L. Zhao, J. Wu, Y. Tu, Y. Zhang, X. Yang, W. Zhang, R. H. Friend, Q. Gong, H. J. Snaith, R. Zhu, *Science* **2018**, *360*, 1442.
- [127] D. Luo, R. Su, W. Zhang, Q. Gong, R. Zhu, *Nat. Rev. Mater.* **2020**, *5*, 44.
- [128] Qi Jiang, Y. Zhao, X. Zhang, X. Yang, Y. Chen, Z. Chu, Q. Ye, X. Li, Z. Yin, J. You, *Nat. Photonics* **2019**, *13*, 460.
- [129] J. Tong, Qi Jiang, A. J. Ferguson, A. F. Palmstrom, X. Wang, Ji Hao, S. P. Dunfield, A. E. Louks, S. P. Harvey, C. Li, H. Lu, R. M. France, S. A. Johnson, F. Zhang, M. Yang, J. F. Geisz, M. D. McGehee, M. C. Beard, Y. Yan, D. Kuciauskas, J. J. Berry, K. Zhu, *Nat. Energy* **2022**, *7*, 642.
- [130] J. Tong, Z. Song, D. H. Kim, X. Chen, C. Chen, A. F. Palmstrom, P. F. Ndione, M. O. Reese, S. P. Dunfield, O. G. Reid, J. Liu, F. Zhang, S. P. Harvey, Z. Li, S. T. Christensen, G. Teeter, D. Zhao, M. M. Al-Jassim, M. F. A. M. van Hest, M. C. Beard, S. E. Shaheen, J. J. Berry, Y. Yan, K. Zhu, *Science* **2019**, *364*, 475.
- [131] Ke Xiao, R. Lin, Q. Han, Yi Hou, Z. Qin, H. T. Nguyen, J. Wen, M. Wei, V. Yeddu, M. I. Saidaminov, Y. Gao, X. Luo, Y. Wang, H. Gao, C. Zhang, J. Xu, J. Zhu, E. H. Sargent, H. Tan, *Nat. Energy* **2020**, *5*, 870.
- [132] W. Ke, C. Chen, I. Spanopoulos, L. Mao, I. Hadar, X. Li, J. M. Hoffman, Z. Song, Y. Yan, M. G. Kanatzidis, *J. Am. Chem. Soc.* **2020**, *142*, 15049.
- [133] F. Zhang, S. Y. Park, C. Yao, H. Lu, S. P. Dunfield, C. Xiao, S. Uličná, X. Zhao, L. Du Hill, X. Chen, X. Wang, L. E. Mundt, K. H. Stone, L. T. Schelhas, G. Teeter, S. Parkin, E. L. Ratcliff, Y.-L. Loo, J. J. Berry, M. C. Beard, Y. Yan, B. W. Larson, K. Zhu, *Science* **2022**, *375*, 71.
- [134] W. Yu, F. Li, T. Huang, W. Li, T. Wu, *Innovation* **2023**, *4*, 100363.
- [135] T. Feng, Z. Wang, Z. Zhang, J. Xue, H. Lu, *Nanoscale* **2021**, *13*, 18925.
- [136] D. D. Awschalom, R. Hanson, J. Wrachtrup, B. B. Zhou, *Nat. Photonics* **2018**, *12*, 516.
- [137] Y.-H. Kim, R. Song, Ji Hao, Y. Zhai, L. Yan, T. Moot, A. F. Palmstrom, R. Brunecky, W. You, J. J. Berry, J. L. Blackburn, M. C. Beard, V. Blum, J. M. Luther, *Adv. Funct. Mater.* **2022**, *32*, 2200454.
- [138] R. M. France, J. F. Geisz, T. Song, W. Olavarria, M. Young, A. Kibbler, M. A. Steiner, *Joule* **2022**, *6*, 1121.